

LiDAR-Based Place Recognition For Autonomous Driving: A Survey

Yongjun Zhang, Pengcheng Shi, Jiayuan Li

Abstract—LiDAR-based place recognition (LPR) plays a pivotal role in autonomous driving, which assists Simultaneous Localization and Mapping (SLAM) systems in reducing accumulated errors and achieving reliable localization. However, existing reviews predominantly concentrate on visual place recognition (VPR) methods. Despite the recent remarkable progress in LPR, to the best of our knowledge, there is no dedicated systematic review in this area. This paper bridges the gap by providing a comprehensive review of place recognition methods employing LiDAR sensors, thus facilitating and encouraging further research. We commence by delving into the problem formulation of place recognition, exploring existing challenges, and describing relations to previous surveys. Subsequently, we conduct an in-depth review of related research, which offers detailed classifications, strengths and weaknesses, and architectures. Finally, we summarize existing datasets, commonly used evaluation metrics, and comprehensive evaluation results from various methods on public datasets. This paper can serve as a valuable tutorial for newcomers entering the field of place recognition and for researchers interested in long-term robot localization. We pledge to maintain an up-to-date project on our website <https://github.com/ShiPC-AI/LPR-Survey>.

Index Terms—SLAM, LiDAR-based Place Recognition, Loop Closure Detection, Map Localization.

1 INTRODUCTION

PLACE recognition [1], [2], [3], [4], [5], [6], [7], [8] is a challenging and ongoing research problem that aims to identify previously visited places across different viewpoints and environments. This task holds great significance in various robotic applications. Firstly, long-term localization [9], [10], [11] and place retrieval [12], [13], [14] address the issue of localization in changing environments. Secondly, place recognition [15], [16], [17], [18] facilitates real-time loop closure detection (LCD) to create drift-free global maps. Thirdly, metric localization [19], [20], [21] within prior maps offers a reliable means to recover the kidnapped vehicle’s poses.

Sensor observation-based methods [22], [23], [24], [25], [26], [27] outperform traditional global positioning system (GPS) [28], [29], [30], inertia measurement unit (IMU) [31], [32], [33], [34], and wheel odometers [35] in autonomy, flexibility, anti-interference capability, independence from geomagnetic signals, and cost-effectiveness. Despite significant research advancements and the emergence of numerous methods in recent years, place recognition remains challenging due to viewpoint differences, occlusions, data variations, long-term changes, and computational complexity. To facilitate and encourage further research, scholars have engaged in method classification [36], performance evaluation [37], [38], challenge summarization [39], and prospect prediction [40] based on the current progress in this field. However, existing work primarily focuses on visual place recognition (VPR), necessitating a comprehensive and systematic review

of LiDAR-based place recognition (LPR) to bridge this gap.

In this paper, we present a comprehensive review of LPR research, accompanied by a detailed methodological taxonomy depicted in Figure 1. We categorize methods into handcrafted and learning-based types, further subdividing them, and present detailed introductions to pioneering works. This well-organized layout enhances reading efficiency and facilitates a better understanding of the relevant technologies in place recognition. Our main contributions are as follows:

- To the best of our knowledge, this paper is the first survey exclusively focusing on place recognition based on 3D LiDAR. We delve into the problem formulation, challenges, and the relationship to previous surveys.
- We provide an in-depth overview of LPR covering conventional handcrafted descriptors and advanced deep-learning techniques. We classify existing methods into seven categories and describe their advantages and limitations.
- We incorporate numerous figures and tables to help readers understand the open-source code, backbone networks, feature types, similarity metrics, memory costs, training strategies, running efficiency, and localization capabilities of these methods.
- We summarize existing datasets and evaluation metrics while comprehensively comparing existing methods on several public datasets. In addition, we also provide a regularly updated project.

The structure of this paper is as follows. Section 1 summarizes our contributions and paper structures. Section 2 describes the research background. From Section 3 to 9, we comprehensively review recent methods and offer detailed classifications. Section 10 collects existing datasets,

This work was supported by the National Natural Science Foundation of China (NSFC) under Grant 42030102 and 42271444, and the Science and Technology Major Project of Hubei Province under Grant 2021AAA010. Yongjun Zhang and Jiayuan Li are with the School of Remote Sensing and Information Engineering, Wuhan University, Wuhan 430079, China. Pengcheng Shi is with the School of Computer Science, Wuhan University, Wuhan 430072, China (Corresponding authors: Pengcheng Shi, Jiayuan Li)

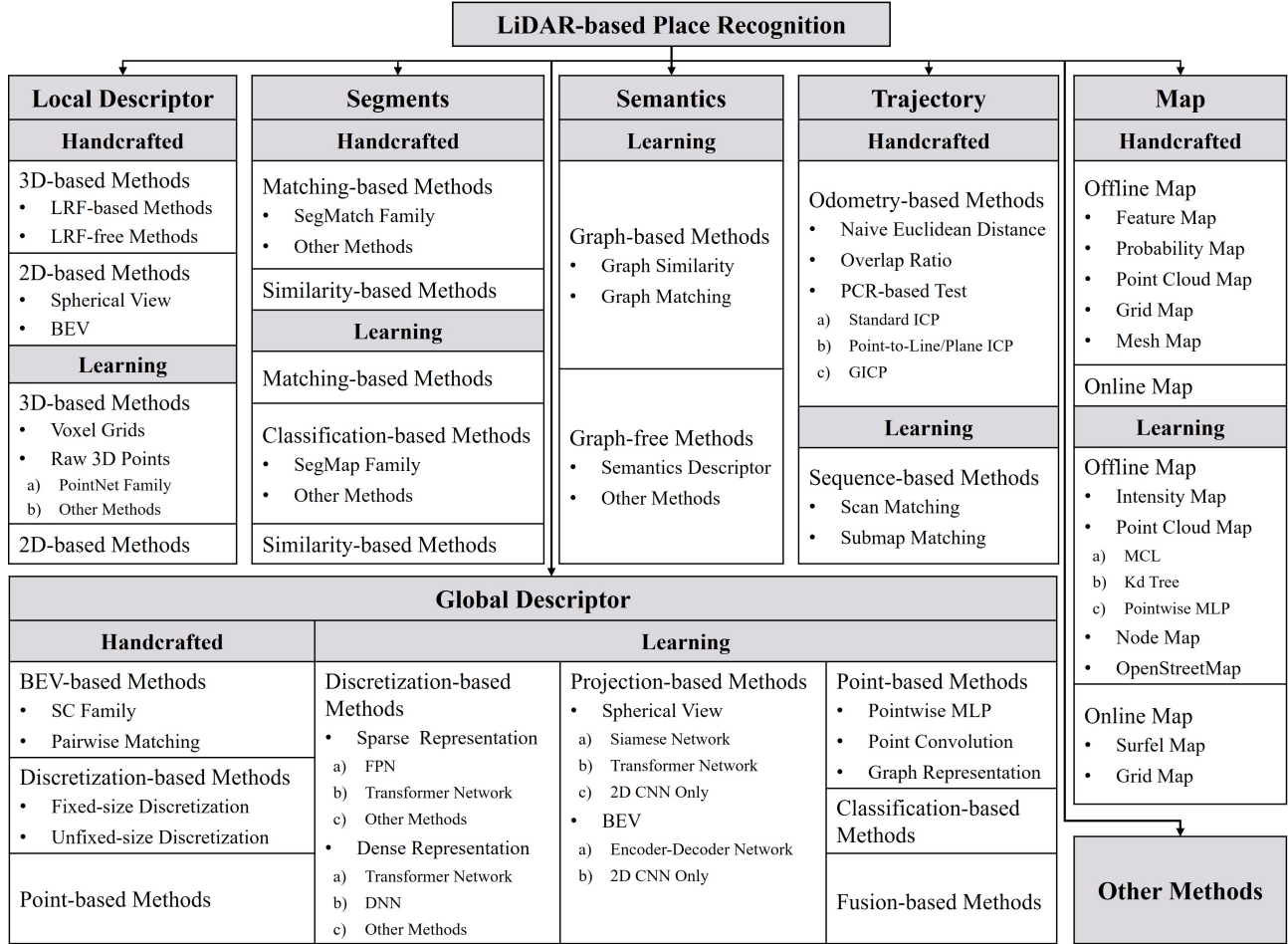


Figure 1: A taxonomy of LPR methods.

evaluation metrics, and performance comparisons on public datasets. Finally, Section 11 presents promising future directions and Section 12 concludes the paper.

2 BACKGROUND

2.1 Problem Formulation

The place recognition task is commonly categorized into three main groups: place retrieval, LCD, and map localization. Given a query data X and reference database D , place retrieval and LCD can be formulated as:

$$\hat{Y} = \arg \max_Y p(X, Y | Y \in D) \quad (1)$$

where Y represents a matching candidate for X and \hat{Y} is the best-matched one. $p(X, Y | X \in D)$ is a similarity or matching score. Place retrieval commonly creates offline databases from pre-collected or generated sequences, while LCD uses real-time simultaneous localization and mapping (SLAM) data for constructing databases.

Map localization involves utilizing a high-definition map (HD Map) and data association techniques to compute the global pose, formulated as:

$$\hat{Y}, \mathbf{T} = \arg \max_Y p(X, Y | Y \in D) \quad (2)$$

where \mathbf{T} is a transformation with six or three degree-of-freedom (DoF). The database D typically comprises prior

map and reference data. This method allows for direct pose comparison, making it applicable in single and multiple robot systems.

2.2 Challenges of LPR

With the advancements in image processing technologies [41] and the availability of affordable equipment, numerous vision-based methods [1], [42], [43], [44] have emerged over the past decades. However, they encounter challenges such as illumination variations, viewpoint changes, adverse weather conditions, and scale ambiguity. In contrast, LiDAR sensors actively emit laser signals to capture high-resolution 3D points, which excel in providing precise and detailed geometric information [45] even in low-light conditions. In addition, the rapid progress of 3D scanning technology further fuels the interest in place recognition research using LiDAR sensors.

Numerous recent LPR methods have explored techniques like bird-eye-view (BEV) [4], [46], [47], histograms [48], [49], image representations [9], [50], and graph theory [51], [52], [53] to enhance performance. They achieve rotational invariance through brute-force search [4], [46] and frequency domain analysis [47], [54]. Additional approaches employ pose proximity [55], [56], sequence matching [6], [57], and point cloud registration (PCR) [58], [59], [60] techniques to improve recognition accuracy. However, these

methods struggle in dynamic and highly occluded environments. Traditional methods rely on low-level features (coordinates [61], normals [62], intensities [63], [64], [65], range [66] and density [67]), while learning-based approaches gradually show promising results using neural networks [68], [69], attention mechanisms [70], [71], semantics [72], [73], and classifiers [74]. Furthermore, diverse map representations, such as point clouds [75], semantics [76], and mesh [77], have been successfully applied in map localization. Despite the impressive results claimed by these methods, several challenges persist that require further attention:

- **Motion Distortions:** The common assumption of constant velocity motion [78], [79] is inaccurate for deskewing distorted scans, especially in high-speed applications.
- **Viewpoint Differences:** Lane-level horizontal deviations may exist when a robot revisits a historical place from different directions. While a few methods [4], [9], [46], [51] address rotation invariance, they overlook the impact of translation on place recognition.
- **Weather Conditions:** Laser signals exhibit varying behavior under different weather conditions [80]. They attenuate less and travel farther on sunny days but decay significantly in rainy and foggy weather.
- **Perceptual Aliasing:** Distinct places in confined corridors [81], [82] may exhibit similar point cloud data, which introduces ambiguous interpretations.
- **Appearance Changes:** Long-term navigation applications [9], [10], [11], [38] often involve significant environmental changes, which leads to potential failures.
- **Sensor Characteristics.** Mechanical LiDAR [58], [83] produces point clouds in a format of multiple scan lines, resulting in vertical sparsity. Solid-state LiDAR [84] provides limited horizontal field-of-view (FOV) and requires specific considerations in the recognition process.

2.3 Relation to Previous Surveys

In recent years, there has been a proliferation of reviews on visual robotics technologies, addressing various topics such as place recognition [36], [37], [39], [40], localization [85], [86], tracking [87], [88], and SLAM [89], [90], [91]. While these reviews have made significant contributions to the progress of research in robotics and autonomous driving, they have regrettably neglected the technology of LiDAR sensors.

Cadena *et al.* [92] extensively reviewed the current state of SLAM and delved into potential future directions. Yin *et al.* [93] provided a comprehensive place recognition survey encompassing cameras, LiDAR, radar, and joint sensors. However, the section dedicated to discussing LiDAR was relatively limited. Yin *et al.* [94] offered an informative overview of the recent progress and advancements in LiDAR-based global localization, while it merely represented a specialized branch of place recognition. Distinct from previous works, our survey solely focused on LiDAR-based place recognition research. It provided a comprehensive overview of the problem formulation, task challenges,

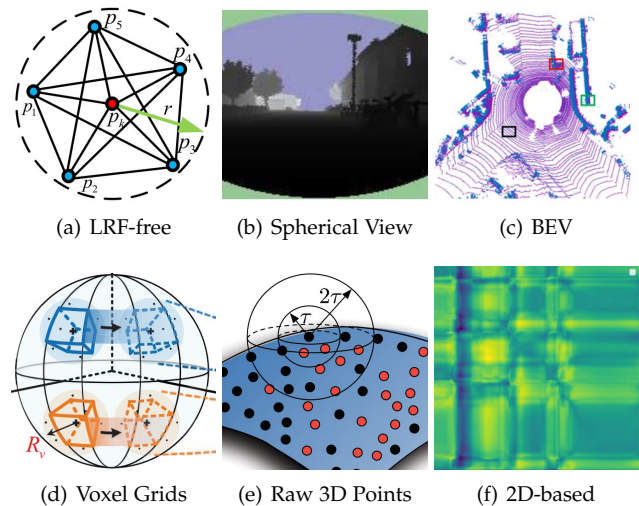


Figure 2: An illustration of local descriptor-based methods. (a)-(f) were originally shown in [100], [106], [49], [115], [119], and [131], respectively. (a)-(c) were handcrafted methods while (d)-(f) were learning-based ones.

method classifications, existing datasets, evaluation metrics, experimental performances, and future directions.

3 LPR TECHNIQUES: LOCAL DESCRIPTOR

The local descriptor is a compact representation of regions or points, capturing distinctive characteristics such as texture, color, density, or shape. Local descriptor-based methods typically extract keypoints and employ local descriptors to characterize their surrounding context. They generally fell into either 3D-based or 2D-based categories based on the nature of descriptors. Table 1 contained a systematic summary. Figure 2 described several representative methods.

3.1 Handcrafted Methods

3.1.1 3D-based Methods

We roughly categorize handcrafted 3D local descriptors into two groups based on a local reference frame (LRF).

LRF-based Methods. LRF aimed to rigidly transform the patch into its canonical representation by selecting neighborhood points to build a covariance matrix and computing the eigenvector as reference axes. While initially designed for PCR, it was also applicable to place recognition. Several methods focused on encoding geometric information, such as normal [63], [103], height [105], and mesh [102], within the LRF to achieve precise geometric descriptions. Others enhanced the stability of LRF using weighted projection vectors [104] or sign disambiguation [101].

LRF-free Methods. Other methods ensured rotation invariance by avoiding LRF construction and focusing solely on the underlying geometry of the local surface. Early methods directly counted surrounding geometric information, such as height [61], distance [3], [97], [98], and density [95], as local surface descriptions. Subsequently, several methods encoded point distribution [96], [100] and sparse triangulated landmark [99].

Table 1: Summary of Handcrafted Local descriptor-based Methods. Handcrafted Methods Were Organized According to the Published Year, Feature Type, Descriptor Size, Similarity Metric, and Code. Learning-based Methods Were Organized According to the Published Year, Backbone Network, Descriptor Size, Loss Function, End-to-end (EtE) Learning, and Code.

Handcrafted Methods								
Methods		Year	Feature	Size	Metric	Code		
3D-based Methods	LRF-free	Spin Image [95]	1999	Density	153	L2 Distance	✓	
		3DSC [96]	2004	Density	1980	L2 Distance	✓	
		PFH [97]	2008	Angle+Distance	125	Kullback-Leibler Distance	✓	
		FPFH [98]	2009	Angle+Distance	33	Euclidean Distance	✓	
		3DGestalt [61]	2013	Height	32×10	Voting		
		NBLD [99]	2016	Density	16×4×8	Voting		
		GLAROT-3D [3]	2017	Orientation+Range	1880	Rotated L1 Norm		
	HoPPF [100]	2020	Angle+Distance	600				
	LRF-based	USC [101]	2010	Density	1960	Euclidean Distance	✓	
		RoPS [102]	2013	Density	135	L2 Distance	✓	
		SHOT [103]	2014	Angle	352	Euclidean Distance	✓	
		TOLDI [104]	2017	Depth	3×20×20			
		ISHOT [63]	2019	Angle+Intensity	1344	Voting	✓	
		Sunet <i>et al.</i> [105]	2020	Height	20×20	Euclidean Distance		
Steder <i>et al.</i> [106]		2010	Range+Curvature		Euclidean Distance			
2D-based Methods	Spherical View	Steder <i>et al.</i> [15]	2011	Range+Curvature	36	Manhattan Distance		
		Zhuang <i>et al.</i> [107]	2013	Space		Matching Score		
		Cao <i>et al.</i> [108]	2018	Position	600×391	L1-Norm		
		Shan <i>et al.</i> [109]	2021	Intensity	1024×128	L1 Distance+Hamming Distance	✓	
		BVMatch [54]	2021	Density	6×6×6	2D Rigid Pose	✓	
		HOPN [49]	2022	Normal+Density	6×6×6	2D Rigid Pose	✓	
	BEV							
	Learning-based Methods							
	Methods		Year	Backbone	Size	Loss	EtE	Code
3D-based Methods	Voxel Grids	3DShapeNet [110]	2015	Convolutional BDN	24×24×24	Contrastive Divergence	✓	
		VolumetricCNN [111]	2016	CNN	512	Classification	✓	
		3DMatch [112]	2017	3D ConvNet	512	Contrastive	✓	
		FCGF [113]	2019	ResUNet	32	Hardest-contrastive and Hardest-triplet		
		3DSmoothNet [114]	2019	CNN	16	Batch Hard	✓	
	Raw 3D Points	SpinNet [115], [116]	2021	Transformer+3DCCN	32	Contrastive	✓	
		PointNet [117]	2017	CNN	1024	Regularization Softmax	✓	
		PointNet++ [118]	2017	PointNet		Cross Entropy	✓	
		CGF [119]	2017	DNN	32	Triples		
		PPFNet [120]	2018	PointNet	64	N-tuple		
		PPF-FoldNet [121]	2018	MLP	512	N-tuple		
		DeepVcp [122]	2019	PointNet++	32	L1+L2	✓	
		RelativeNet [123]	2019	PPF-FoldNet		Chamfer	✓	
		D3feat [124]	2020	KPConv		Contrastive+Triplet	✓	
		L3Ds [125]	2022	TNet+PointNet	32	Contrastive	✓	
		Poesiet <i>et al.</i> [126]	2022	QNet+PointNet++	32	Hardest-contrastive	✓	
		LEAD [127]	2022	Spherical CNN	512	Chamfer Distance	✓	
		LORAX [25]	2017	DNN	1032	Pixel-wise Error+ICP	✓	
		2D-based Methods	MVDesc [128]	2018	MatchNet	32	Double-margin Contrastive	
			Li <i>et al.</i> [129]	2020	CNN	32	Batch-hard triplet	✓
Gojic <i>et al.</i> [130]	2020		FCGF	32	Hardest Contrastive	✓		
DeLightLCD [131]	2022		DNN	1×300×32	Binary Cross Entropy	✓		

3.1.2 2D-based Methods

These methods projected a point cloud to a 2D image and built handcrafted local descriptors from the image, followed by an image matching problem. Spherical view and bird-eye-view (BEV) were two representative projection approaches.

Spherical View. Projecting point clouds into a spherical or range image using a bearing angle (BA) model effectively mitigated orientation ambiguity. Steder *et al.* [106] pioneered the projection of point clouds to range images for place recognition. They extracted the local descriptor vector [132] and evaluated candidate transformations through keypoint reprojection. Afterward, several works extended the method [106] using normal aligned radial features (NARF) [15], speeded up robust features (SURF) [107] and ORB [108], [109].

BEV. Several works incorporated proposal-wise features from BEV images into image matching. BVMatch [54] extracted the maximum index map [133] of the Log-Gabor filter responses, employing BEV feature transform and BoW for place recognition. This approach provided relative poses

and effectively overcame sparsity and intensity distortion. Luo *et al.* [49] applied features from accelerated segment test (FAST) [134] detectors on the BEV image and constructed a HOPN descriptor using 3D normals. It showcased superior localization capability in large-scale scenarios.

3.2 Learning-based Methods

3.2.1 3D-based Methods

Learning-based 3D local descriptors typically employ 3D CNNs to encode point cloud patches, divided into voxel grids and raw 3D points according to network inputs.

Voxel Grids. The pioneering work 3DMatch [112] transformed patches into voxel grids of truncated signed distance function (TSDF) and employed eight convolutional layers to learn local descriptors. Subsequently, several works extended this idea to more informative encoding manner such as binary occupancy [111], multi-label occupancy [110], sparse tensor representation [113], smoothed density value [114], and spherical voxelization [115], [116].

Raw 3D Points. An alternative method involved direct processing of the raw point cloud data.

1) *PointNet Family*. PointNet [117] was a pioneering work of learning from unordered point clouds, which learned a symmetry function approximated by a multi-layer perceptron (MLP) to handle detailed shapes. Subsequently, PointNet++ [118] introduced an enhanced version that used ball query search to apply PointNet [117] recursively and aggregated features from multiple scales. Several works extended PointNet [117] by normals [120], FoldingNet decoder [121], orientation [123], LRF [125], [126], and semantics [122].

2) *Other Methods*. Compact Geometric Features (CGF) [119] trained a deep network to map from the high-dimensional space of spherical histograms to a low-dimensional Euclidean space. D3Feat [124] designed a dual-role fully convolutional network that densely predicted both detection scores and description features. Local equivariant descriptor (LEAD) [127] combined spherical CNNs to learn the equivariant representation and utilized plane-folding decoders for unsupervised learning.

3.2.2 2D-based Methods

Several works inferred local descriptors using well-established 2D CNNs from projected 2D images. They demonstrated superior performance in the task of 3D shape recognition and retrieval. LORAX [25] and DeLightLCD [131] employed a deep neural network (DNN) auto-encoder and attention to enhance descriptor descriptiveness on 2D depth images, respectively. Another spectrum of research fused multi-view features into local descriptors by soft-view pooling [129], graphical model [128], and spectral relaxation [130].

3.3 Summary

This section reviewed some representative methods and more comprehensive surveys of local descriptors were available in [135], [136], [137]. Although local descriptors found wide applications in tasks such as PCR and object recognition, they were not the preferred methods for place recognition. There were mainly the following reasons:

- Viewpoint changes could affect the accuracy of 3D keypoints [138], rendering them unsuitable for matching. Moreover, they might not effectively handle data noise and object occlusions.
- The usage of 3D local descriptors [61], [99] could be challenging as it required dense point clouds, which was computationally expensive and might not work well with sensors like Velodyne VLP-16 [66] that produced sparse point clouds.
- While converting point clouds into images [54], [106], [131] could use mature image processing techniques, this resulted in the loss of geometric information, making it unsuitable for large-scale scenarios.

4 LPR TECHNIQUES: GLOBAL DESCRIPTOR

The global descriptor captures the overall features of a scene, providing a holistic view of the data rather than focusing on specific regions or points. Table 2 contains a systematic summary of global descriptor-based methods.

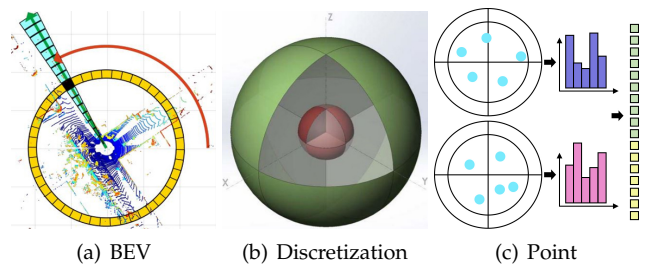


Figure 3: An illustration of handcrafted global descriptors. (a) and (b) were originally shown in [4] and [64], respectively.

4.1 Handcrafted Methods

Handcrafted global descriptors usually used a single descriptor to describe the entire point cloud. According to the type of space division, they could be divided into BEV-based, discretization-based, and point-based methods. Three representative methods were shown in Figure 3.

4.1.1 BEV-based Methods

BEV projection gained significant attention in the robotics community due to its ability to enhance algorithm efficiency through dimension reduction, making it highly suitable for real-time applications. Scan Context (SC) [4] family and pairwise matching were two mainstream methods.

SC Family. As illustrated in Figure 3(a), the pioneering work SC [4] partitioned the horizontal space into discrete bins while maintaining the points' maximum height to generate a 2D matrix descriptor. It utilized the ring key to search for potential matches and conducted a column-wise comparison to identify the closest one. This method demonstrated promising performance but might fail when dealing with significant lateral offsets. Subsequently, researchers proposed a series of SC-based variant methods, which employed the polar and cart context [7], intensities [46], [140], frequency domain [144], local reference frame (LRF) [139], F-norm [143], and spatial binary pattern (SBP) [145] to enhance performance. Furthermore, certain studies [175], [176], [177] had incorporated SC-based methods into the LCD module of LiDAR SLAM frameworks to enhance the performance of localization and map construction.

Pairwise Matching. LiDAR Iris [47] drew inspiration from human iris signatures, utilizing LoG-Gabor filtering and thresholding to create binary signature images, then measuring descriptor similarities using Hamming distance. Some methods also employed weighted distances [67] and orientation-invariant metrics [141], [142] for pairwise similarity computation.

4.1.2 Discretization-based Methods

The discretization processing transformed the point cloud into 3D discrete representations, categorized into fixed and unfixed size-based approaches.

Fixed-size Discretization. Magnusson *et al.* [146] mapped the point cloud to normal distribution transform (NDT) voxels and created a histogram based on the probability density function of the local surface. They calculated the descriptor similarities using weighted

Table 2: Summary of Global Descriptor-based Methods. Handcrafted Methods Were Organized According to the Published Year, Similarity Metric, Descriptor Size, Feature Type, and Code. Learning-based Methods Were Organized According to the Published Year, Backbone Network, Feature Aggregator, Descriptor Size, Loss Function, and End-to-end (EtE) Learning.

Handcrafted Methods								
Methods		Year	Metric	Size	Feature	Code		
BEV		SC [4]	2018	L0 Norm+Cosine Distance	60×20	Height	✓	
		ISC [46]	2020	Cosine Distance	60×20	Intensity		
		LiDAR Iris [47]	2020	Hamming Distance	80×360	Height	✓	
		Shi <i>et al.</i> [139]	2021	Cosine Distance	60×20	Height		
		WSC [140]	2021	Cosine Distance+Euclidean Distance		Height+Intensity		
		SC++ [7]	2021	L1 Norm+Cosine Distance	60×20	Height	✓	
		RING [141]	2022	Circular Cross-correlation	120×120	Occupancy		
		RING++ [142]	2022	Circular Cross-correlation	120×120	Height+Occupancy	✓	
		FSC [143]	2022	F-Norm		Height+Intensity		
		PGHCI [67]	2022	JS Divergence+Pixel Values	40×20	Height		
Discretization		FreSCo [144]	2022	L1 Norm+Cosine Distance	20×120	Height	✓	
		Ou <i>et al.</i> [145]	2023	Cosine Distance	5×20×60	Density+Height		
		Magnusson <i>et al.</i> [146]	2009	Euclidean Distance		Shape		
		DELIGHT [64]	2018	Chi-squared Test	256	Intensity		
		Lin <i>et al.</i> [84]	2019	Normalized Cross-correlation	60×60	Shape	✓	
Point		Mo <i>et al.</i> [147]	2020	L2-Norm+Chi-square Test	192+256+60×20	Density+Intensity+Height	✓	
		Cao <i>et al.</i> [148]	2021	Euclidean Distance	360×180	Context+Layout		
		Z-Projection [62]	2011	χ^2 Distance+Sørensen Distance	101	Normal		
		Fast Histogram [48]	2015	Wasserstein Metric	80	Height		
Learning-based Methods		M2DP [149]	2016	L2-Norm	192	Density	✓	
		C-M2DP [150]	2019	L2 Distance	576	Color+Shape		
Learning-based Methods								
Methods		Year	Backbone	Aggregator	Size	Loss	EtE	
Point	Pointwise MLP	Pointnetvlad [12]	2018	PointNet	NetVLAD	256	Lazy triplet and quadruplet	✓
		PCAN [70]	2019	PointNet	NetVLAD	256	Lazy quadruplet	✓
		SOE-Net [151]	2021	PointNet	NetVLAD	256	HPHN quadruplet	✓
		LCD-Net [152]	2022	PV-RCNN	NetVLAD	256	Triplet	✓
	Point Convolution	DH3D [71]	2020	FlexConv+SE block	NetVLAD	256	N-tuple	✓
		EPC-Net [69]	2022	PPCNN	VLAD	256	Lazy quadruplet	
	Graph	LPD-Net [5]	2019	PointNet	NetVLAD	256	Lazy quadruplet	✓
		DAGC [13]	2020	ResGCN	NetVLAD	256	Lazy quadruplet	✓
		SR-Net [153]	2020	SGC+SAM	NetVLAD	1024	Lazy quadruplet	✓
		vLPD-Net [154]	2021	LPD-Net+S-ARN	MinkPool		Joint loss	
Discretization	Sparse Volumetric	PPT-Net [155]	2021	Transformer	VLAD	256	Lazy quadruplet	
		MinkLoc3D [156]	2021	FPN	GeM	256	Triplet margin	
		MinkLoc++ [157]	2021	ResNet18+FPN	GeM	256	Triplet margin	
		EgoNN [158]	2021	CNN	GeM	256	Triplet margin	
		TransLoc3D [159]	2021	Transformer	NetVLAD	256	Triplet margin	✓
		MinkLoc3Dv2 [160]	2022	FPN	GeM	256	Modified Smooth-AP	
		MinkLoc3D-SI [161]	2022	FPN	GeM	256	Triplet margin	
		SVTNet [8]	2022	Transformer	GeM	256	Triple	
	Dense Discretization	LoGG3D-Net [162]	2022	U-Net	O2P+ePN	256	Contrastive+Quadruplet	✓
		SpoxelNet [163]	2020	CNN	NetVLAD		Lazy quadruplet	✓
Projection	Spherical View	VBRL [164]	2020				Modality norm	
		HiTPR [165]	2022	Transformer	Max pooling	1024	Lazy quadruplet	
		NDT-Transformer [166]	2022	Transformer	NetVLAD	256	Lazy quadruplet	✓
		Yin <i>et al.</i> [167]	2017	DNN			Contrastive	
		MMCS-Net [168]	2022	Siamese CNNs	NetVLAD		Contrastive	✓
		SeqOT [169]	2022	Transformer	GeM	256	Triplet	✓
	BEV	OverlapTransformer [170]	2022	Transformer	NetVLAD	256	Lazy triplet	✓
		AttDLNet [171]	2021	DarkNet53	Max pooling	1024	Cosine similarity	
		OREOS [50]	2019	CNN			Triplet	
		SCI [9]	2019	LeNet			Categorical cross-entropy	✓
Fusion	DisCO [68]		2021	U-Net		1024	Quadruplet+KL divergence	✓
		PIC-Net [172]	2020	Resnet50+PointNet	NetVLAD	512	Lazy quadruplet	
	CORAL [18]	2021	ResNet18+FPN	NetVLAD	256	Lazy quadruplet	✓	
	Bernreiter <i>et al.</i> [173]	2021	Spherical CNN			Triplet	✓	
	Adafusion [174]	2022	CNN	GAP	256	Pairwise margin	✓	

Euclidean distances. This method demonstrated the potential of NDT descriptors for place recognition. Subsequently, researchers introduced techniques like k-means++ clustering [178] and normalized cross-correlation metrics [84], [179] to enhance generalization. Cao *et al.* [148] also generated a numerical descriptor by detecting contours and computing spectrum energies from wedge-shaped voxels.

Unfixed-size Discretization. As depicted in Figure 3(b), DELIGHT [64], [147] divided the support region into two concentric spheres and got non-overlapping bins by horizontal and azimuthal divisions. It computed intensity histograms for each bin and assessed descriptor similarities by

chi-squared tests. Notably, the descriptor could be local or global based on the descriptor’s radius and center point.

4.1.3 Point-based Methods

Several methods treated place recognition as a histogram matching problem, encoding angle [62] and height [48] information and calculating histogram similarities using Wasserstein metric [48], Sørensen [62], and χ^2 distances [62]. They achieved rotation invariance and overcame noises. As shown in Figure 3(c), a parallel track of works followed a projection-based scheme. M2DP [149] and C-M2DP [150] projected the point cloud onto multiple 2D planes using azimuth and elevation angles, counting point density

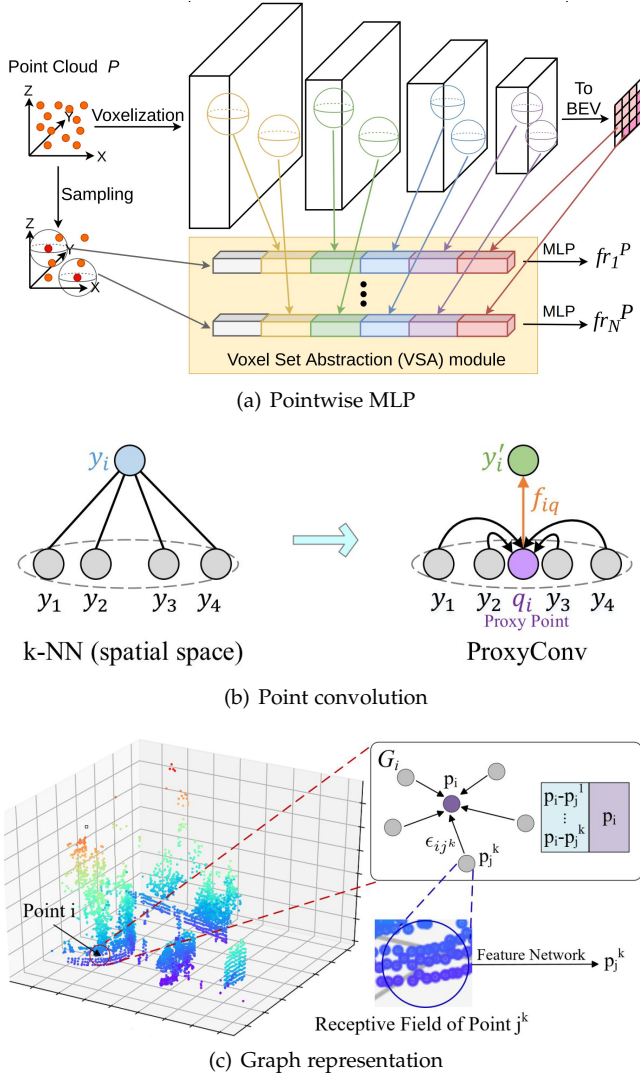


Figure 4: An illustration of point-based methods. (a)-(c) were originally shown in [152], [69], and [5], respectively

attributes to create the descriptor. Computing multi-view density signatures enabled accurate descriptions with fewer computational resources, making it particularly effective for sparse point clouds.

4.2 Learning-based Methods

This section explored learning-based methods for obtaining global descriptors, categorized into five groups based on network architecture and model mechanism: point-based, discretization-based, classification-based, projection-based, and fusion-based methods.

4.2.1 Point-based Methods

One prevalent approach directly utilized the inherent 3D spatial information for LiDAR point cloud processing, involving point-wise MLP, point convolution, and graph representation, as shown in Figure 4.

Pointwise MLP. The pioneering end-to-end work PointNetVLAD [12] combined PointNet [117] for local feature extraction and NetVLAD [43] for global descriptor generation. It employed metric learning [180] and introduced the

lazy triplet and quadruplet loss functions to enhance the generality of global descriptors. Afterward, PCAN [70] and SOE-Net [151] improved high-dimensional feature representation by incorporating attention mechanisms. As depicted in Figure 4(a), LCD-Net [152] utilized the PointVoxel-RCNN (PV-RCNN) [181] architecture and combined the feature extraction capabilities of deep neural network with transport theory algorithms.

Point Convolution. DH3D [71] introduced a Siamese network for local feature detection, description, and global descriptor extraction in a single forward pass. It incorporated multi-level spatial contextual information and channel-wise feature correlations using flex convolution (FlexConv) [182] and squeeze-and-excitation (SE) [183]. As shown in Figure 4(b), EPC-Net [69] was a compact model based on edge convolution, simplifying the process with spatial-adjacent matrices and proxy points. It achieved excellent performance while significantly reducing computational memory.

Graph Representation. Graph networks efficiently capture underlying geometric and shape properties, allowing for effective processing and feature comparison across multiple locations within graphs. As illustrated in Figure 4(c), LPD-Net [5] and vLPD-Net [154] combined adaptive local feature extraction with a graph-based neighborhood aggregation module. They extracted multiple local features, including curvature, height, and density, and employed a graph neural network (GNN) for feature aggregation. Several works integrated an attention module to discern task-relevant features [13], learn spatial relationships between regions [155], and mitigate the influence of movable noises [153].

4.2.2 Discretization-based Methods

We divided discretization-based methods into sparse and dense representations based on voxel density.

Sparse Representation. Three approaches for generating global descriptors using 3D CNNs on sparse volume representations were feature pyramid network (FPN), transformer network, and other methods.

1) *FPN.* MinkLoc3D [156], a pioneering work based on sparse voxelization, employed a 3D FPN [184] architecture and generalized-mean (GeM) [185] pooling for global descriptor generation. It showcased a simple and elegant architecture, highlighting the potential of sparse voxelized representation and sparse convolutions for efficient 3D feature extraction. Later works extended MinkLoc3D [156] by incorporating intensity [161], image [157], and attention [158], [160] to enhance recognition performance.

2) *Transformer Network.* TransLoc3D [159] re-weighted features from multiple receptive scales using an attention map and incorporated external attention layers for capturing long-range contextual information. SVT-Net [8], illustrated in Figure 5(a), introduced two types of transformers to capture short-range local features and long-range contextual features, respectively. Despite a shallow network architecture, it generated descriptive descriptors.

3) *Other Methods.* LoGG3D-Net [162] utilized sparse U-Net [186] for high-dimensional feature embedding and introduced a local consistency loss for feature similarity max-

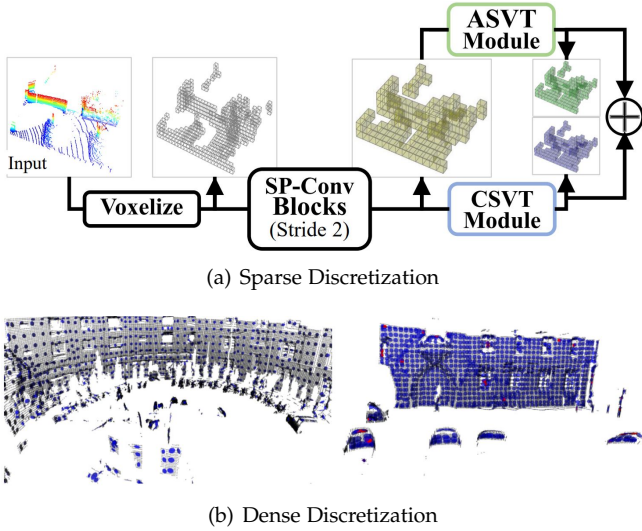


Figure 5: An illustration of discretization-based methods. (a) and (b) were originally shown in [8] and [166], respectively.

imization. It exhibited superior end-to-end performance, operating in near real-time.

Dense Representation. Likewise, we broadly categorized dense representation-based approaches into transformer network, DNN, and other methods.

1) *Transformer Network.* HiTPR [165] utilized a short-range transformer to extract local features within cells and a long-range transformer to encode global relations among the cells. It enhanced the relevance of local neighbors and global contextual dependencies, showcasing its superior effectiveness. As shown in Figure 5(b), NDT-Transformer [166] introduced a novel network with three stacked transformer encoders, learning a global descriptor from discrete NDT cells. It struck a valuable balance between state-of-the-art (SOTA) performance and runtime, making it a valuable addition to NDT-based SLAM and MCL methods.

2) *DNN.* SpoxelNet [163] voxelized the point cloud in spherical coordinates, representing voxel occupancy using ternary values. It extracted multi-scale structural features and generated a global descriptor by concatenating features from various directions. This method effectively handled occlusion and moving objects in crowded indoor spaces.

3) *Other Methods.* Voxel-based representation learning (VBRL) [164] tackled long-term place recognition by jointly learning voxel importance and feature modalities using structured sparsity-inducing norms. It integrated all features into a unified regularized optimization formulation.

4.2.3 Classification-based Methods

Several approaches addressed the place recognition problem using classifiers. FastLCD [65] encoded multi-modality features into a global descriptor, detecting candidate loop closures using supervised learning and rejecting false positives through cross-validation and post-verification. On the other hand, Habich *et al.* [187] used a compact global descriptor [188] to encode each LiDAR scan, performed loop searches within a variable radius based on the largest eigenvalue of the position covariance matrix and predicted loop events using an AdaBoost [189] classifier.

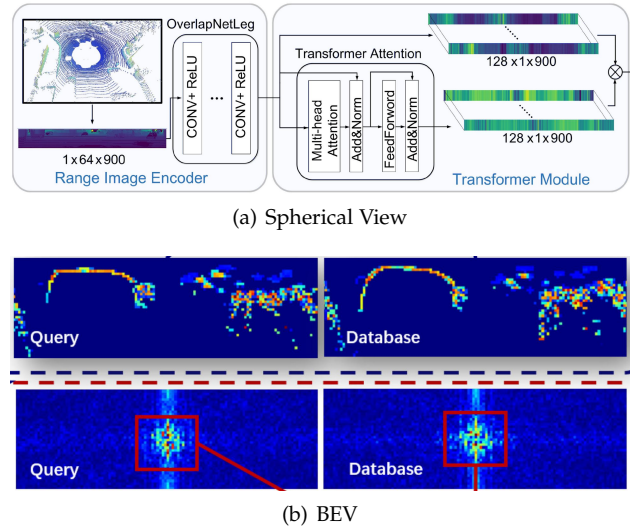


Figure 6: An illustration of projection-based methods. (a) and (b) were originally shown in [170] and [68], respectively.

4.2.4 Projection-based Methods

Following the taxonomy of learning-based 2D local descriptors (Section 3.1.2), this section also categorized projection methods into spherical view and BEV.

Spherical View. Using spherical projection images as input, three representative methods included siamese network, transformer network, and 2D CNN only.

1) *Siamese Network.* Yin *et al.* [167] transformed the point cloud into a one-channel image using range distribution and spherical coordinates. They used a Siamese CNN to convert LCD into a similarity modeling problem, improving search efficiency by combining Euclidean metric and kd-tree. MMCS-Net [168] incorporated a Siamese CNN with shallow-deep feature fusion and a cascaded attention mechanism to handle pseudo images. It effectively encoded targeted features for challenging scenes, striking a favorable balance between effectiveness and efficiency.

2) *Transformer Network.* SeqOT [169] employed multi-scale transformers to generate sub-descriptors that fuse spatial and temporal information from sequential LiDAR range images. The yaw-rotation-invariant architecture ensured robustness to viewpoint changes and scan order, enabling reliable place recognition even in opposite directions. As depicted in Figure 6(a), OverlapTransformer [170] applied a modified OverlapNetLeg to extract features from range images and integrated a transformer module to capture relative feature locations and global information. It demonstrated fast running speed and robust generalization across diverse environments. Attention-based deep learning network (AttDLNet) [171] also incorporated a four-layer attention network to capture long-range context and inter-feature relationships.

3) *2D CNN Only.* OREOS [50] used 2D convolutional and max pooling layers to extract features from 2D range images, enhancing the descriptor performance via a triple loss function and strong negative mining strategy. It efficiently computed the descriptor while enabling long-term 3-DoF metric localization in outdoor environments.

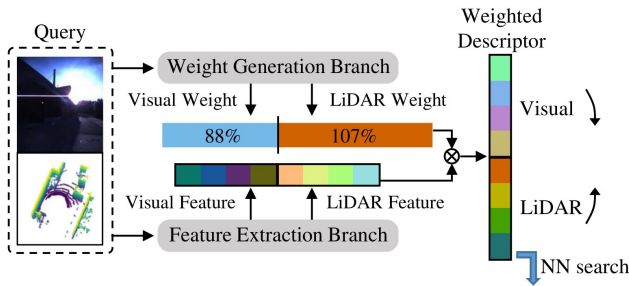


Figure 7: An illustration of fusion-based methods [174].

BEV. Two representative BEV-based methods were encoder-decoder network and 2D CNN only.

1) *Encoder-Decoder Network.* As shown in Figure 6(b), differentiable scan context with orientation (DiSCO) [68] employed an encoder-decoder network to extract descriptors and estimated relative orientation through Fourier-Mellin Transform and differentiable phase correlation. It enhanced the interpretability and efficiency of the feature extractor.

2) *2D CNN Only.* Scan context image (SCI) [9] extended SC [4] into three channels, enabling robot localization on a grid map through a convolutional neural network-based place classification. It demonstrated robust year-round localization with only a single day of learning.

4.2.5 Fusion-based Methods

These methods combined LiDAR and image features to enhance descriptor capabilities. Several works transformed the point cloud into an image and only utilized a 2D network for descriptor extraction. CORAL [18] used ResNet18 [190] to extract multi-scale features from elevation and visual images. Bernreiter *et al.* [173] employed spherical CNNs [191], [192], [193] to learn a multi-modal descriptor from spherical and visual images. As depicted in Figure 7, another line of research involved employing both 2D and 3D networks. Adafusion [174] and PIC-Net [172] incorporated an attention mechanism to learn adaptive feature weights and created a compound descriptor using two types of networks.

4.3 Summary

Global descriptors were currently the most popular place recognition method, which could provide information about the entire scene, unaffected by local changes. The progress of deep learning in 3D computer vision paved the way for data-driven methods in LPR. Several observations were summarized as follows:

For the handcrafted part:

- BEV [4], [7], [46], [140] demonstrated superior performance in flat structural environments but has three main limitations: (1) When the z-axis of the LiDAR changed in the global coordinate system, poor results might arise because these methods assumed local planar vehicle motion. (2) Large lateral offsets might cause missed loops or failed re-localization. (3) Rotation matching could only compute yaw angles, leading to potential local optimum issues if used as initial poses for iterative closest point (ICP) [194].

- Discretization-based methods [84], [146], [148] could describe the local surface using robust mathematical theories. However, increasing the resolution would significantly incur a heavy computational burden.
- Point-based methods [48], [62], [149], [150] were the most basic global descriptor methods. However, they required expensive neighbor searching to establish topological relationships. Furthermore, projection operations [149], [150] might result in information loss and cause potential false positives.

For the learning part:

- Learning-based methods delivered impressive efficiency and accurate recognition but heavily relied on ample training samples and extensive data cleaning. Real-world environments presented additional challenges, including noise, occlusions, and uncertainties in LiDAR measurements. Consequently, transfer learning might be necessary for specific applications.
- Transformers [165], [166], [169], [170], [171] excelled at capturing long-range dependencies and contextual relationships, enabling reliable recognition in cluttered environments. However, their substantial computational demands constrained the batch size for metric learning.
- Sparse convolutional architectures [156], [157], [160], [161] excelled at generating informative local features while struggling to discriminate feature size in dynamic scenarios. Additionally, simply stacking convolution layers might neglect long-range contextual information.
- Point-based methods [5], [12], [13], [70], [71], [151] were permutation invariant and could handle unordered point clouds but lacked explicit capture of local spatial relationships. Classification-based methods [65], [187] assigned higher weights to informative features during training, emphasizing discriminative features. However, the specific contribution of each weak classifier to the overall prediction might be less interpretable.
- Projection-based methods [9], [50], [68], [168] had lower computational complexity and offered more interpretable results. However, they might suffer from information loss due to dimensionality reduction. Fusion-based methods [18], [173], [174] harnessed the complementary strengths of different sensors. Nevertheless, achieving consistent data association in dynamic environments remained challenging.

5 LPR TECHNIQUES: SEGMENTS

Segments are meaningful region divisions characterized by similar geometric properties. These methods divide the point cloud into segments and three representative methods are shown in Figure 8.

5.1 Handcrafted Methods

These approaches generally extracted segment features for place recognition and could be divided into matching-based and similarity-based methods.

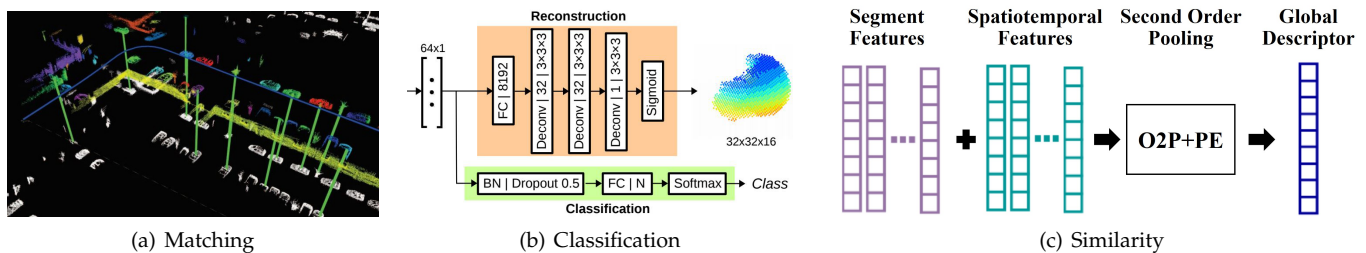


Figure 8: An illustration of three representative segment-based methods. (a)-(c) were originally shown in [74], [195], and [196], respectively.

5.1.1 Matching-based Methods

Segment-based matching for finding correspondences primarily comprised the SegMatch [74] family and other methods.

SegMatch Family. The pioneering work SegMatch [74], depicted in Figure 8(a), employed Euclidean clustering to partition the point cloud into segments and extracted eigenvalue-based features. It effectively identified potential correspondences using random forest and random sample consensus (RANSAC) [197]-based geometric verification. Dubé *et al.* [198] enhanced SegMatch [74] by tracking a single segment using region-growing-based incremental segmentation. Moreover, certain studies effectively integrated SegMatch [74] into traditional LiDAR SLAM [199] and multi-robot systems [200].

Other Methods. DL-SLAM [201] employed k-means to extract segments from a 2.5D heightmap and defined five descriptors to facilitate segment matching. RDC-SLAM [202] combined an eigenvalue-based segment descriptor, k nearest neighbors (KNN) search, and RANSAC-based verification [197] to refine relative poses. It accurately fused information from multiple robots without prior knowledge. Gong *et al.* [203] constructed a spatial relation graph to represent segments, effectively capturing general spatial relations between irregular clusters.

5.1.2 Similarity-based Methods

Seed [204] developed a segmentation-based egocentric descriptor, incorporating topological information into SC-based place recognition [4]. It achieved translation and rotation invariance by utilizing the inner topological structure of segmented objects.

5.2 Learning-based Methods

Neural network application on segments primarily involved matching, classification, and similarity computation.

5.2.1 Matching-based Methods

Tinchev *et al.* [205] encoded geometric properties and point distribution of segments to extract repeatable oriented key poses, which were matched using reliable shape descriptors and a Random Forest. However, significant changes in the sensor's vantage point could negatively impact segment-matching performance. Tinchev *et al.* [206] utilized convolution [207] to obtain an embedding space suitable for urban and natural scenarios. They subsequently estimated match quality through probabilistic geometric validation.

5.2.2 Classification-based Methods

Several works computed the category of segments by performing classification in the descriptor space, categorized into SegMap [195], [208] family and other methods.

1) *SegMap Family.* As shown in Figure 8(b), the pioneering work SegMap [195], [208] incrementally clustered point clouds to create a global segment map. It employed segment-wise KNN retrieval with a data-driven descriptor extractor comprising three convolutional and two fully connected layers, then assigned a classification score using a fully connected network. It enabled high compression rates in environment reconstruction and facilitated large-scale 3D LiDAR SLAM. Subsequently, researchers successfully integrated SegMap [195] into LiDAR SLAM [209] and segment-based mapping framework [210].

2) *Other Methods.* Wietrzykowski *et al.* [211] proposed a DNN that improved segment-based descriptors by learning visual context from synthetic LiDAR intensity images. They claimed that using the latest LiDAR and ambient images could yield additional performance improvements. OneShot [66] employed a range image-based method [212] for segment extraction and a custom-tailored neural network to extract LiDAR-Vision descriptors.

5.2.3 Similarity-based Methods

Another approach constructed segment-based descriptors and assessed their similarities, thus combining the advantages of segments and global descriptors. Deep scan context (DSC) [213] introduced egocentric segmentation for computing eigenvalues and centroids of segments, employing a GNN to aggregate these features into a descriptor. It outperformed traditional Euclidean clustering in efficiency and robustness for sparse point cloud processing. As shown in Figure 8(c), Locus [196] encoded topological and temporal information of segments to create a global descriptor using second-order pooling and nonlinear transformation. It avoided global map pooling construction and segment-wise KNN search, achieving robustness to viewpoint changes and occlusions.

5.3 Summary

Traditional point cloud descriptors relied on low-level properties [46], [48], [62], [64], [106] to encode the point cloud, but local descriptors lacked description ability, and global descriptors struggled with rotation and translation invariance. Fortunately, segments offered a good compromise between the two. Several observations were summarized as follows:

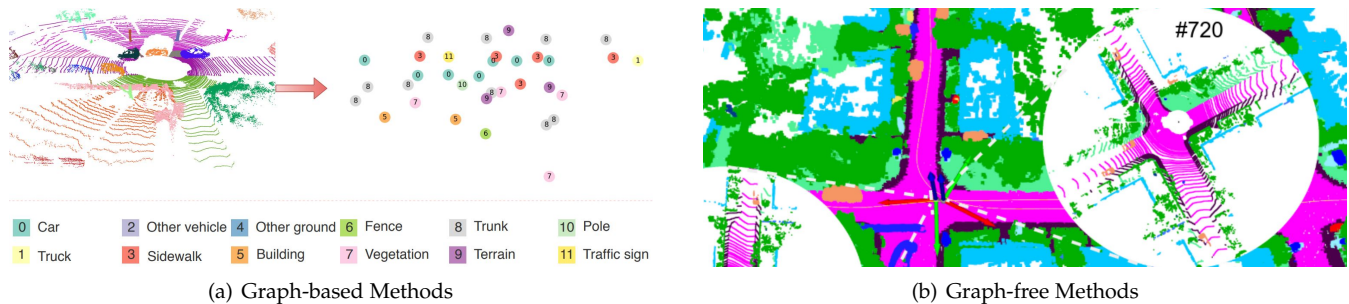


Figure 9: An illustration of semantics-based methods. (a) and (b) were originally shown in [51] and [73], respectively.

- Segments [74], [195], [208], [210] offered a potential solution to reduce feature computation by avoiding processing the entire point cloud. Nevertheless, several approaches relied on point cloud aggregation or map construction, leading to inefficiencies when dealing with large-scale environments.
- Segment-based methods showed promise in enhancing accuracy by incorporating geometric, color, and semantic information of segments. However, they required rich 3D geometry structures for segmentation, which might not always be available, thus limiting their applicability.
- Segment-based methods were well-known for their resilience to environmental changes, encompassing illumination, weather, and seasonal variations. However, they offered limited insights into the underlying 3D structures, resulting in subpar segmentation performance during long-term localization scenarios with numerous moving objects.

6 LPR TECHNIQUES: SEMANTICS

Semantics refers to labels or categories that divide point clouds into various instances using learning-based segmentation technology, facilitating semantic-level place recognition. Thus, semantics-based place recognition falls under the category of learning-based methods. Based on the approach used for semantics association, they can be classified into two types: graph-based and graph-free.

6.1 Learning-based Methods

6.1.1 Graph-based Methods

Semantic graphs intuitively depicted the location and topological information of objects. Graph similarity and graph matching were two typical graph operations.

Graph Similarity. X-view [214] computed random walk descriptors for each graph node and determined the similarity score based on the count of identical random walks. It was general in semantic input and mitigated high computational expenses. As depicted in Figure 9(a), SGPR [51], [53] represented semantic categories and centroids of points as nodes, capturing node feature relations through edges. It developed a GNN-based graph network with node embedding, graph embedding, and graph-graph interaction to compute graph similarity. SGPR demonstrated robustness against occlusion and viewpoint changes, especially for reverse loops.

Graph Matching. GOSMatch [52] introduced an object-based place recognition approach for urban environments, which employed graph descriptors for candidate search and vertex descriptors for one-to-one correspondence calculation. BoxGraph [215] stored object shapes in vertices and simplified place recognition to an optimal vertex assignment problem. It employed bounding boxes as appearance embeddings for vertex entities and extended them for pose estimation.

6.1.2 Graph-free Methods

Other works avoided semantic graph construction and mainly fell into two categories: semantic descriptors and other methods.

Semantic Descriptors. As shown in Figure 9(b), semantic scan context (SSC) [73], [216] enhanced SC [4] by utilizing semantics [217] instead of height. Object scan context (OSC) [218] improved SC [4] by constructing the descriptor around uniformly distributed objects (e.g., street lights and trash cans). It made the descriptor independent of LiDAR’s position and overcame the issue of distant point clouds. SeqNdt [219] extended the NDT-based histogram descriptor [220] by incorporating semantic information and utilized the kullback-leibler (KL) divergence to measure similarity. RINet [221] developed a lightweight siamese network with convolution, down-sampling, and attention mechanisms to compute descriptor similarities. It prioritized scene learning over point cloud orientation and was highly efficient, allowing for deployment on resource-constrained platforms.

Other Methods. Recent studies enhanced semantic-based LPR through innovative technologies and theories, including multiple hypothesis trees [222], siamese neural network [72], [223], [224], spherical convolution [225], and neural tensor network [226].

6.2 Summary

Inspired by human perception, semantics-based methods utilized pre-defined knowledge databases to categorize objects and identify their topological relationships. However, these methods were still relatively new and immature because they required advanced semantic segmentation technology. Several key observations were summarized below:

- Graph-based methods [51], [52], [53], [215] had streamlined point cloud comprehension but exhibited three limitations: (1) Potential loss of specific features, like object size. (2) Inability to differentiate

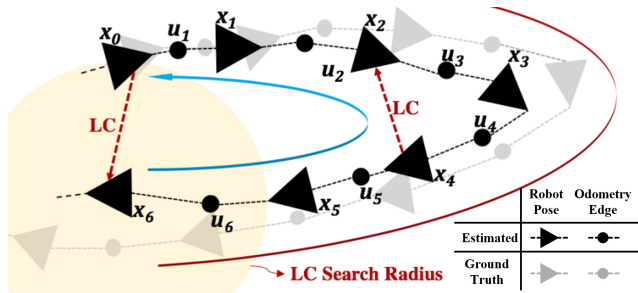


Figure 10: An illustration of odometry-based methods [227].

between parts of the same category leading to information loss. (3) Computing metrics between two graphs remains NP-complete, hindering the precise distance calculation within a reasonable timeframe.

- Semantic labels [217] outperformed using only geometric features, offering more interpretable and intuitive results. They demonstrated greater resilience to occlusion and viewpoint changes, especially in reverse LCD. However, predefined semantic labels in test datasets were limited, failing to encompass various categories in real-life scenarios.
- In dynamic or cluttered environments, leveraging objects and their topological information could enhance recognition accuracy. These methods heavily relied on the outcomes of semantic segmentation, which might lead to poor performance in diverse scenarios. Despite these challenges, they held promise in applications where traditional methods fell short.

7 LPR TECHNIQUES: TRAJECTORY

Trajectory information enables correlating current and recent historical scans for place recognition. Odometry (handcrafted) and sequence (learning) are two prominent usage methods for historical data.

7.1 Odometry-based Methods

SLAM systems with LCD modules often adopt handcrafted approaches, utilizing front-end poses or traditional registration techniques for place recognition to reduce system complexity. They could be further categorized into naive Euclidean distance, overlap ratio, and PCR-based test.

7.1.1 Naive Euclidean Distance

Comparing the Euclidean distance between real-time and historical poses enabled rough loop closure detection. Some works use piecewise orientation functions [228] and global factor graphs [55] for pose similarity comparison, while others employ multi-sensor calibration and mapping [229].

7.1.2 Overlap Ratio

The overlap ratio could assess place similarity, with a higher value indicating closer proximity. S4-SLAM [230] implemented a location-based LCD by storing historical poses using a kd tree and evaluating candidate loops based on overlap rate. This approach balanced real-time performance and accuracy, demonstrating robustness even with limited feature points and high moving speeds. Mendes *et al.* [231]

utilized an overlap criterion to generate new keyframes and implemented a graphical model layer over LiDAR odometry to reduce drifts through graph-level loop closing. The hard rejection based on normal angles effectively prevented unexpected drifts arising from vegetation.

7.1.3 PCR-based Test

PCR techniques verified candidate loops using relative poses, such as standard ICP, point-to-line/plane ICP, and generalized ICP (GICP).

Standard ICP. IN2LAAMA [232] devised an offline probabilistic framework covering localization, mapping, and calibration. It identified loop closures using poses and validated candidates with an optional ICP test ICP [194], proficiently handling motion distortion without an explicit motion model.

Point-to-Line/Plane ICP. Lego-LOAM [58] calculated odometry poses using a two-step Levenberg-Marquardt optimization, comparing historical scans with pose constraints and refining transformations with ICP [194]. It was pioneering work to incorporate LCD into LiDAR SLAM, making it well-suited for long-duration navigation tasks. Subsequently, LILO [56] extended this idea to a LiDAR-IMU system. Other works enhanced registration robustness using plane graphs [233], intuitive weighting [234], and KL divergence [235], respectively.

GICP. As shown in Figure 10, LAMP [227] developed a multi-robot LiDAR SLAM system for challenging subterranean environments that utilized GICP [236] to register nearby scans and proposed an incremental consistent measurement (ICM) set maximization [237] to reject outlying loop closures. Similarly, LAMP 2.0 [238] combined TEASER++ [239] and GICP [236] to compute the relative transform and filter poor matches. SPC-SLAM [240] leveraged the geometric-rigidity-constant assumption [241] and submap registration score [236] to confirm loop closure, addressing high-precision mapping challenges in GNSS-denied environments.

7.2 Sequence-based Methods

SeqSLAM [243] pioneered visual feature similarity comparisons over time to integrate sequence information and identify the best match within local sequences, showcasing exceptional performance in extreme environmental changes and providing insights for LiDAR-based solutions. The point cloud sequence matching incurred higher computational costs than image-based alternatives. Consequently, approaches such as scan matching and submap matching integrated neural networks with GPUs to enhance efficiency.

7.2.1 Scan Matching

As shown in Figure 11(a), SeqLPD [242] employed LPD-Net [5] for global descriptor extraction and selected super keyframes based on feature space distribution. It combined super keyframe-based coarse matching with the local sequence fine matching to improve detection accuracy and efficiency. This method achieved advanced performance without relying on odometry data. The trained model could be directly applied in real-world scenarios without additional training, facilitating practical applications.

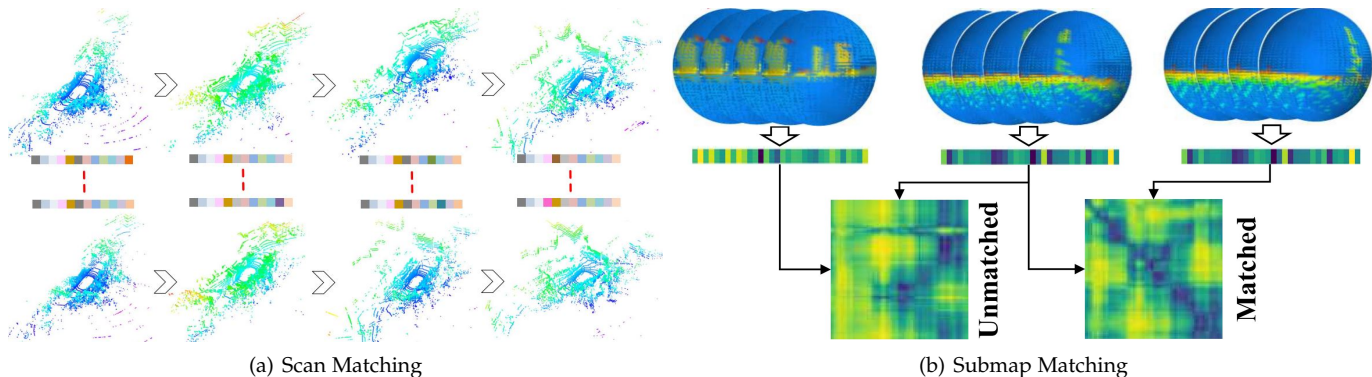


Figure 11: An illustration of sequence-based methods. (a) and (b) were originally shown in [242] and [6], respectively.

7.2.2 Submap Matching

Chen *et al.* [244] integrated LPD-Net [5] with sequence-based matching and introduced a plane-driven sub-maps matching algorithm to computed relative transformations. This method employed interval stabbing for translation search, demonstrating nearly real-time computation capabilities. As illustrated in Figure 11(b), SeqSphereVLAD [6] and Yin *et al.* [57] utilized a spherical convolution module to extract orientation-equivariant local features across multiple layers of spherical perspectives. It effectively handled changing viewpoints and addressed large-scale SLAM challenges. FusionVLAD [245] proposed a multi-view fusion network that encoded top-down and spherical-view features from the local map, enhancing feature combination through a parallel fusion module for end-to-end training. It was well-suited for large-scale mapping tasks with limited computation resources.

7.3 Summary

Traditional frame-to-frame comparison methods yielded an intuitive similarity score but intended to degrade in closed, symmetric, and dynamic environments. The trajectory-based approaches incorporated both spatial and temporal information to address this limitation. Two observations were summarized as follows:

- LiDAR SLAM [227], [240] employed a straightforward LCD method based on pose proximity, followed by PCR for calculating relative transformations. Despite satisfactory results, two limitations remained: (1) Cumulative errors affected the reliability of odometry poses in large-scale scenarios. (2) The local optimality of PCR impeded the integration of loop constraints into global optimization.
- Sequence-based methods exhibited versatility since they effectively incorporated diverse place recognition techniques, such as local and global descriptors [57], [242], semantics, and segments. While visual sequence-based methods had been well-studied, LiDAR-based approaches were still in the early stages. Furthermore, the expensive calculations required for matching and feature fusion restricted their practical applicability.

8 LPR TECHNIQUES: MAP

Map-assisted methods provided global metric localization to achieve place recognition. They generally fall into two groups based on the map construction timing: offline and online maps. Figure 12 illustrates several representative maps.

8.1 Handcrafted Methods

8.1.1 Offline Map-based Methods

As the vehicle moved, the static offline map confined its motion within predefined boundaries. Handcrafted methods mainly involved five map types: feature, probability, point cloud, grid, and mesh.

Feature Map. Dong *et al.* [10] employed range image-based pole extraction to build a global map and utilized monte carlo localization (MCL) to update particle weights based on pole matching. It demonstrated accurate pole extraction in diverse environments, improving long-term localization performance. Shi *et al.* [81] combined RANSAC [197] and Euclidean clustering to extract walls from the offline map and online scans, applying point-to-point and point-to-line distance constraints to compute vehicle poses.

Probability Map. As depicted in Figure 12(a), Schmiedel *et al.* [22] characterized surface patches in NDT maps using curvature and object shape. They matched descriptors between online scans and the global map, applied RANSAC [197] for outlier detection, and evaluated matches using a normalized inlier ratio.

Point Cloud Map. Xu *et al.* [75] introduced a cross-section shape context (CSSC) descriptor that described spatial distribution using elevation and point density, improving recognition performance with two-stage similarity estimation and the nearest cluster distance ratio. As depicted in Figure 12(b), Shi *et al.* [82], [249] created an offline map database with a kd tree to simulate vehicle orientations and developed a binary loss function to improve localization accuracy.

Grid Map. As shown in Figure 12(c), Aldibaja *et al.* [246] converted LiDAR scans into image-like representations of road surfaces, incorporating elevation and irradiation data. They employed a shared ID-based XY correlation matrix to represent loop-closure events among map nodes, facilitating large-scale map processing and map-combiner event detection independent of the driving trajectory.

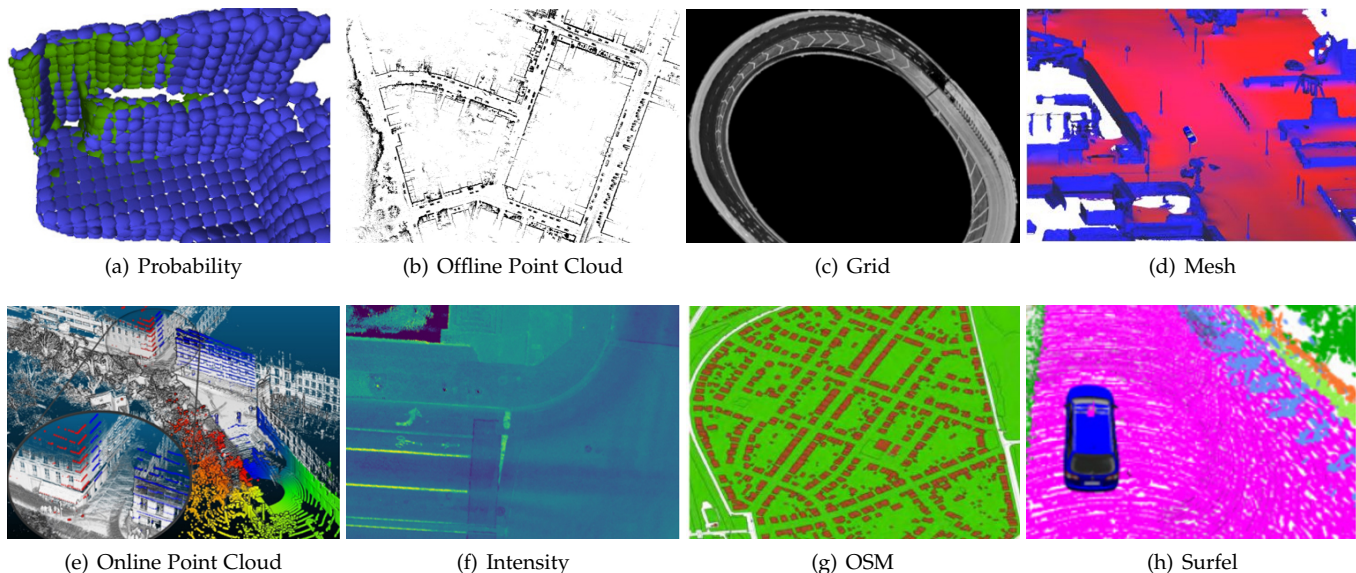


Figure 12: An illustration of four types of maps. (a)-(h) were originally shown in [22], [59], [77], [82], [246], [247], [248] and [76], respectively. (a)-(d), (f), and (h) were offline while (e) and (g) were online.

Mesh Map. As depicted in Figure 12(d), Chen *et al.* [77] employed Poisson surface reconstruction to generate a mesh map, developing an observation model of an MCL framework. It showcased robust generalization across different LiDAR sensors, eliminating the need for additional training data in varying environments.

8.1.2 Online Map-based Methods

SLAM dynamically constructed and updated an online point cloud map of the surrounding environment as the vehicle navigated within unknown terrain. As illustrated in Figure 12(e), Multi-metric linear least square (MULLS) [79] incorporated TEASER [239] for loop verification and employed map-to-map ICP [194] to enhance inter-submap edges with accurate transformations. Continuous-time ICP (CT-ICP) [59] projected a local map onto an elevation image, estimated a 2D transformation using RANSAC [197], and computed a 6-DoF pose through ICP [194] to identify potential loop closures. Liu *et al.* [250] introduced a real-time 6D SLAM for large-scale natural terrains, which combined rotation histogram matching with a branch and bound search-based ICP [194] to achieve real-time LCD.

8.2 Learning-based Methods

8.2.1 Offline Map-based Methods

Researchers explored three types of offline maps in learning-based map localization: intensity, point cloud, and node.

Intensity Map. As shown in Figure 12(f), Barsan *et al.* [247] embedded LiDAR intensity maps and online scans into a joint space, using efficient convolutional matching to determine the vehicle’s position. This method achieved centimeter-level accuracy, showcased robustness in handling uncalibrated data, and successfully generalized across various LiDAR sensors.

Point Cloud Map. Three representative methods in this context were monte carlo localization (MCL), kd tree, and pointwise MLP.

1) **MCL.** LocNet [19], [251] introduced a semi-handcrafted DNN and MCL framework for global localization, utilizing a Gaussian mixture model to represent multiple hypotheses of place recognition. Leveraging learned representations and vehicle poses, it constructed a prior map, achieving high accuracy and efficiency for long-term localization. Sun *et al.* [252] combined efficient deep deterministic model inference with rigorous geometry verification using a Bayes-filter approach, resolving the non-conjugacy issue between Gaussian and MCL.

2) **Kd Tree.** Jin *et al.* [253] incorporated the D3feat descriptor [124] with a self-supervised detector loss for feature matching. They employed a kd tree to store map descriptors and improved search efficiency through a coarse-to-fine voting mechanism and a two-phase search strategy.

3) **Pointwise MLP.** L3-Net [26] utilized a mini-PointNet for feature descriptor extraction and regularized the cost volume with 3D convolutions. It computed matching probabilities for optimal estimation and captured temporal motion dynamics through deep recurrent neural networks (RNNs). L3-Net achieved comparable localization accuracy to SOTA methods and was well-suited for multi-sensor fusion. Retriever [14] extracted compact features through an encoder and feature propagation network, aggregating them with a perceiver for place recognition in compressed point cloud maps. It improved computing efficiency by avoiding computation-heavy decompression.

Node Map. S4-SLAM2 [254] constructed a node map comprising point cloud data, feature vectors, and location information. It extracted geometric and statistical features to create multi-modal descriptors and classified loop closures with a random forest classifier.

OpenStreetMap. OSM, a global open-source map, offered comprehensive geographic details such as streets, railways, water systems, and buildings. Ruchti *et al.* [255] created a road network and categorized environments as road or non-road, leveraging this classification to weight

MCL particles. Several approaches [256], [257] integrated semantic information extracted from OSM into a particle filter framework. As depicted in Figure 12(g), Cho *et al.* [248] generated a descriptor by calculating the distances to buildings at regular angles.

8.2.2 Online Map-based Methods

These methods were roughly divided into surfel-based and grid map-based methods.

1) *Surfel Map*. As depicted in Figure 12(h), SuMa [258] and SuMa++ [76] employed range images and surfel-based maps for data association, detecting candidate loops by combining radius search and frame-to-model ICP [194] registration. They verified loops by tracking poses, which ensured robust detection even with low overlap and yielded globally consistent maps.

2) *Grid Map*. Yin *et al.* [259] generated a BEV map from the local occupancy map, considering vehicle motion errors. Furthermore, they introduced an additional GAN [260] with conditional entropy reduction to enhance unsupervised feature learning for long-term recognition applications.

8.3 Summary

Maps [26], [82], [252] had been widely used in robot localization and path planning as they offered precise and detailed representations of the environment. Remarkably, map-based methods excelled in recognizing topologically similar localization, providing pose information, and recovering kidnapped robots effectively. Several observations were summarized as follows:

- Map representations enhanced global consistency and reduced localization errors. However, their large memory requirements resulted in time-consuming loading, communication, and processing.
- Map-based methods could overcome noise and partial occlusions, ensuring robust recognition even in challenging scenarios. However, the significant density difference posed difficulties in registering online scans to maps.
- A robust prior map facilitated long-term robot localization in a consistent environment. However, significant environmental changes could cause the existing map to be outdated, resulting in localization and recognition errors.

9 LPR TECHNIQUES: OTHER METHODS

InCloud [271] distilled the angular relationship between global representations, preserving the complex structure of the embedding space between training steps. It effectively addressed catastrophic forgetting, allowing models to update with new domains without retraining the network on all legacy data. Granström *et al.* [188] encoded the point cloud using geometry features and range histograms, detecting loops with a trained AdaBoost [189] classifier. While achieving high precision and recall rates, this method required the ordered point cloud.

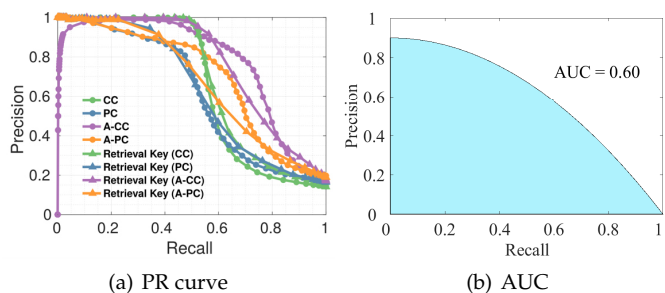


Figure 13: An illustration of PR curve and AUC. (a) was originally shown in [7]. The AUC in (b) corresponded to the area of the blue region.

10 BENCHMARKING

In this section, we summarized existing datasets and evaluation metrics while comparing existing methods on public datasets.

10.1 Datasets

A large number of datasets had been collected to evaluate the performance of LPR methods. Table 3 provided a summary of these datasets. Their characteristics were summarized as follows:

Long-term Collection. [263], [264], [269] repeatedly gathered the same scenario along similar routes in different seasons or times.

Multi-modal Data. In addition to LiDAR sensors, radar was used in [267], [269] and cameras were mounted in [170], [225], [261], [262], [263], [264], [268], [269], [270]. Semantic information was also available in [266].

LiDAR Sparsity. These datasets covered various density LiDAR sensors, such as mechanical 16-line [265], [268], 32-line [263], [269], 64-line [261], [262], and 128-line LiDAR [143], as well as solid-state LiDAR [84].

Viewpoint Change. In addition to same-direction revisits, [143], [148], [168], [170], [262], [263], [264], [265], [266], [267], [268], [269], [270] contained reverse loops.

Scenario Diversity. These datasets were generally divided into two categories: indoor and outdoor datasets. Outdoor datasets were the most widely used, mainly including campuses [263], highways [265], rural areas [262], cities [268], and riversides [267].

10.2 Evaluation Metrics

Different evaluation metrics had been proposed to test LPR methods, summarized as follows:

Revisit Criteria. A distance threshold was defined before evaluation to determine whether the query and candidate belonged to the same place.

Precision-recall (PR) Curves [272]. As depicted in Figure 13(a), this curve measured the relationship between precision (P) and recall (R) under different threshold parameters. P measured the ratio of correct matches to the total of predicted positive instances, while R quantified the proportion of real positive cases correctly identified as positive matches:

$$P = \frac{TP}{TP + FP} \quad (3)$$

Table 3: A Summary of Existing Datasets for LPR. Seq, GT and LT Represented the Sequence, Ground-truth, and Long-term, Respectively. S and O Represented the Same and Oppo-direction Loop, Respectively.

Year	Name	Seq	Trajectory (KM)	Type	Sensor Modility	Model of LiDAR	Loop	GT	LT	Public
2009	Hannover2 [146]	1	1.24	Outdoor	LiDAR		S+O	✓		✓
2010	Freiburg [106]	1	0.723	Outdoor	LiDAR	SICK LMS	S	✓		✓
2011	Ford Campus [261]			Outdoor	Camera+LiDAR	Velodyne HDL-64E		✓		✓
2012	KITTI Odometry [262]	22	39.2	Outdoor	Camera+LiDAR	Velodyne HDL-64E	S+O	✓		✓
2016	NCLT [263]	27	147.4	Indoor+Outdoor	Camera+LiDAR	Velodyne HDL-32+Hokuyo UTM-30LX+Hokuyo URG-04LX	S+O	✓	✓	✓
2017	Oxford RobotCar [264]	> 130	>1000	Outdoor	Camera+LiDAR	SICK LD-MRS+SICK LMS-151	S+O	✓	✓	✓
2018	Complex Urban [265]	19	158.82	Outdoor	LiDAR	Velodyne VLP-16+SICK LMS-511	S+O	✓		✓
2018	In-House [12]	3		Outdoor	LiDAR	Velodyne HDL-64E		✓	✓	✓
2019	Semantic KITTI [266]	22	39.2	Outdoor	LiDAR	Velodyne HDL-64E	S+O	✓		✓
2019	Apollo-SouthBay [26]		>380	Outdoor	LiDAR	Velodyne HDL-64E		✓	✓	✓
2020	MulRan [267]	12	41.2	Outdoor	LiDAR+Radar	Ouster OS1-64	S+O	✓	✓	✓
2020	USyd [268]	>50		Outdoor	Camera+LiDAR	Velodyne VLP-16	S+O	✓	✓	✓
2020	Oxford Radar Robotcar [269]	>32	>280	Outdoor	Camera+LiDAR +Radar	Velodyne HDL-32E+SICK LMS-151+Navtech CTS350-X	S+O	✓	✓	✓
2021	DUT-AS [148]	30		Outdoor	LiDAR	SICK LMS 511	S+O	✓	✓	
2021	CMU Dataset [225]	11	2.0	Outdoor	Camera+LiDAR	Velodyne VLP-16		✓		
2021	Pittsburgh Dataset [225]	12	12.0	Outdoor	Camera+LiDAR	Velodyne VLP-16		✓		
2022	HAOMO [170]	5		Outdoor	Camera+LiDAR	HESAI PandarXT-32	S+O	✓	✓	✓
2022	Campus [57]	11	2	Outdoor	LiDAR	Velodyne-VLP 16		✓		
2022	City [57]	13	11	Outdoor	LiDAR	Velodyne-VLP 16		✓		
2022	KITTI-360 [270]	9	73.7	Outdoor	Camera+LiDAR	Velodyne HDL-64E	S+O	✓		✓
2022	CHDloop [143]	5	1.519	Outdoor	LiDAR	RoboSense RS-Ruby 128	S+O	✓		
2019	HKUST [84]			Indoor+Outdoor		Livox-MID40				✓
2022	LGSVL [168]			Outdoor		Velodyne HDL-64E		✓	✓	
2022	Real Vehicle [168]			Outdoor	Camera+LiDAR	Velodyne VLP-32C	S+O	✓		

$$R = \frac{TP}{TP + FN} \quad (4)$$

where TP , FP , and FN represented true positive, false positive, and false negative, respectively.

Area Under the PR Curve (AUC) [9], [72]. As illustrated in Figure 13(b), it reflected the discrimination power of a place recognition method and a larger AUC meant more places were recognized with fewer errors. However, it did not retain any information regarding the features of the original PR Curve.

Recall @Top-N. It evaluated the accuracy of place recognition methods in identifying the correct places among the top-k retrieved matches. A higher value indicated better performance. TOP 1% [54] and TOP 1 [141] were the two most frequently used metrics.

F_β Score. It was the harmonic mean of precision and recall. A high value indicated the system struck a good balance between them as follows:

$$F_\beta = (1 + \beta^2) \times \frac{P \times R}{\beta^2 P + R} \quad (5)$$

where P and R represented precision and recall, respectively. β was a parameter that determined the weights of recall and precision. F_1 score [51], [65], [72], [73], [196], [203], [213], [215] was the most frequently used metric:

$$F_1 = 2 \times \frac{P \times R}{P + R} \quad (6)$$

where F_1 treated P and R as equally important. The maximum F_1 score (F_1^m) was then calculated as:

$$F_1^m = \max_{\tau} 2 \times \frac{P_{\tau} \times R_{\tau}}{P_{\tau} + R_{\tau}} \quad (7)$$

where the variable parameter τ could assume different roles, e.g., an algorithm parameter, a threshold representing the same place, or the number of retrieved candidates.

Extended Precision (EP). It provided more comprehensive insights by simultaneously considering the lower and upper-performance bounds of an LPR method [73], [196], [213], [273]:

$$EP = \frac{1}{2} (P_{R0} + R_{P100}) \quad (8)$$

where P_{R0} was the precision at minimum recall, and R_{P100} was the max recall at 100% precision.

Running Efficiency. Runtime was crucial for online SLAM systems. Descriptor-based methods typically involved feature extraction and search, while map-based methods required map processing and matching. Data-driven methods, on the other hand, necessitated training and inference.

10.3 Evaluation Results

To facilitate researchers in comprehending the performance of each method, we extensively gathered experimental evaluations on public datasets. As summarized in Table 4, we collected the publish year, method type, code, source of results, maximum F_1 score, EP [273], and runtime on KITTI Odometry [262]. Furthermore, Table 5 mainly summarized the publish year, code, source of results, average recall (AR), runtime, and parameter size of learning-based methods on Oxford [264] and In-house [12] datasets.

The KITTI Odometry evaluations revealed that LocuS [196], Gong *et al.* [203], BoxGraph [215], RINet [221], and LoGG3D-Net [162] achieved F1 scores exceeding 0.97 in multiple sequences. In terms of EP accuracy, BoxGraph

Table 4: Evaluation Results (Maximum F_1 , EP, and Runtime) on KITTI Odometry [262] Dataset. H and L Represented Handcrafted and Learning-based Methods, Respectively. Source Represented the Source of Results. EP Referred to Extended Precision [273].

Year	Method	Type	Code	Source	Maximum F_1						EP						Time (ms)
					00	02	05	06	07	08	00	02	05	06	07	08	
2015	Fast Histogram [48]	H		[19], [170]	0.44	0.43				0.46							2
2016	M2DP [149]	H	✓	[73], [149]	0.71	0.72	0.60	0.79	0.56	0.07	0.62	0.60	0.61	0.68	0.59	0.50	366
2018	PointNetVLAD [12]	L	✓	[73]	0.78	0.73	0.54	0.85	0.63	0.04	0.64	0.69	0.54	0.77	0.59	0.50	
	SC [4]	H	✓	[73]	0.75	0.78	0.90	0.97	0.66	0.61	0.61	0.63	0.80	0.92	0.55	0.57	5
	SuMa [258]	H		[223], [258]		0.85											48
	SuMa++ [76]	L	✓	[76]							0.70	0.29					
2019	LPD-Net [5]	L		[131]		0.85											23
2020	ISC [46]	H	✓	[73]	0.66	0.71	0.77	0.84	0.64	0.41	0.63	0.61	0.73	0.82	0.64	0.54	4
	SGPR [51]	L	✓	[51], [73]	0.82	0.75	0.75	0.66	0.87	0.75	0.50	0.50	0.53	0.50	0.72	0.52	9
	OverlapNet [72], [223]	L	✓	[73], [170]	0.87	0.83	0.92	0.93	0.82	0.37	0.56	0.64	0.80	0.74	0.59	0.50	3238
	LocNet [19]	L		[19]	0.70	0.60				0.70							
	LocNet- Δr [19]	L		[19]	0.68	0.70				0.68							
2021	NDT-Transformer [166]	L	✓	[170]		0.85											16
	MinkLoc3D [156]	L	✓	[170]		0.87											24
	Locus [196]	L	✓	[213], [221]	0.98	0.76	0.98	0.99	1.00	0.93	0.83		0.92	0.91	0.83	0.74	1210
	SSC-RN [73]	L	✓	[73]	0.94	0.89	0.94	0.99	0.87	0.88	0.83	0.75	0.90	0.97	0.77	0.73	5
	SSC-SK [73]	L	✓	[73]	0.95	0.89	0.95	0.99	0.88	0.94	0.85	0.75	0.90	0.97	0.81	0.93	5
	DiSCO [68]	L	✓	[221]	0.96	0.89	0.96	0.99	0.90	0.90							4310
	Gong <i>et al.</i> [203]	L		[203]	1.00	0.94	0.99	1.00	0.99	0.97							448
	LiDAR Iris [47]	H	✓	[47], [73]	0.67	0.76	0.77	0.91	0.63	0.48	0.63	0.67	0.75	0.79	0.65	0.56	231
	AttDLNet-E3A4 [171]	L	✓	[171]	0.94	0.82	0.90	1.00	1.00	0.75							20
	AttDLNet-E5A4 [171]	L	✓	[171]	0.95	0.69	0.86	0.99	0.10	0.72							20
	2022	BG-RN [215]	L		[215]	0.99	0.97	0.96	1.00	1.00	0.79	0.99	0.93	0.95	0.99	1.00	0.79
BG-SK [215]		L		[215]	1.00	0.96	0.97	1.00	1.00	0.96	0.99	0.89	0.97	1.00	1.00	0.93	
SC-LPR [226]		L	✓	[226]	0.97	0.95	0.93	0.99	0.99	0.88							224
SC-LPR-K [226]		L	✓	[226]	0.93	0.93	0.93	0.99	0.99	0.83							224
RINet-CY [221]		L	✓	[221]	0.98	0.95	0.92	0.98	0.97	0.87							211
RINet-SK [221]		L	✓	[221]	0.99	0.95	0.95	1.00	1.00	0.96							211
DSC [213]		L		[213]	0.88	0.84	0.78	0.86	0.82	0.85	0.70	0.68	0.63	0.73	0.58	0.65	50
OverlapTransformer [170]		L	✓	[170]		0.88											2
LOGG3D-Net [162]		L	✓	[162]	0.95	0.89	0.98	0.98	1.00	0.84							90
CSSC [75]		H	✓	[75]	0.37		0.76			0.56							
CSSC-TS [75]		H	✓	[75]	0.91		0.93			0.90							
DeLightLCD [131]		L		[131]		0.90											2

[215], SSC [73], and Locus [196] exhibited the best performance. For the Oxford RobotCar dataset, MinkLoc++ [157], TransLoc3D [159], and MinkLoc3Dv2 [160] achieved an average recall (@%1 and @1) surpassing 95%. Similarly, MinkLoc3D [156], TransLoc3D [159], SVT-Net [8], ASVT-Net [8], CSVT-Net [8], and MinkLoc3Dv2 [160] achieved an average recall of over 93% on In-house datasets.

11 FUTURE DIRECTIONS

In this section, we present several promising trends for future evolution to promote and facilitate further research.

11.1 Multi-modality Information

Multi-modality information offers the opportunity to leverage complementary features and enhance the robustness of place recognition and localization. Several novel solutions are as follows:

WiFi. WiFi-based localization retrieves the media access control (MAC) address of routers via the client device (e.g., cellphone) to calculate positions. This solution offers extensive coverage and achieves accurate indoor localization, overcoming GPS signal limitations. Moreover, it is easy to deploy and provides fast localization, holding significant potential for advancing indoor localization industries.

Voice. Voice-based localization uses microphone arrays to capture audio signals, employing delay estimation or spectral analysis to determine sound source locations. It offers advantages like low computational requirements, high concealment, and strong compatibility. Furthermore, it can

seamlessly integrate with human-computer interaction systems, smart homes, and other voice-controlled applications, enhancing vehicle situational awareness.

Radio Frequency Identification (RFID). RFID employs radio signals to identify and track objects without physical contact. Its anti-interference capability will ensure reliable autonomous driving in harsh environments. Additionally, the long lifespan can enhance the stability of long-term localization systems. Applying cryptographic encryption to tag data can strengthen system security.

11.2 Innovative Solutions

Breaking free from conventional solutions and incorporating interdisciplinary new technologies into autonomous driving holds the potential for unforeseen improvements:

Cloud Computing. Cloud computing offers high-performance shared computing resources to users. Offloading computing tasks to cloud servers enhances robot localization efficiency. With access to powerful computing resources, robots can process diverse high-precision sensor data, thus improving their localization capabilities.

Quantum Technology. Quantum technology revolutionizes information calculation, encoding, and transmission. Quantum sensors can capture subtle changes, delivering ultra-high-precision measurements. Integrating such sensors into robotic navigation will greatly enhance localization and mapping in complex environments.

Bio-inspired Localization. Bio-inspired navigation and group behavior provide novel insights for robot localization. Inspired by turtles' navigation behavior, robots can enhance

Table 5: Evaluation Results (AR @1 and @1%, Runtime, and Parameter Size) of Learning-based Methods on Oxford RobotCar (Oxford) [264] and In-house Datasets [12] Including University Sector (U.S.), Residential Area (R.A.), and Business District (B.D.). AR Referred to the Average recall. Baseline Represented That the Network Was Trained Using Oxford [264] Dataset, While Refine Represented That the Network Was Trained Using Oxford [264] and In-house [12] Datasets. Source Represented the Source of Results. Paras Denoted the Size of Parameters.

Year	Method	Code	Source	Oxford		U.S.		R.A.		B.D.		Time (ms)	Paras (Mb)	
				@1%	@1	@1%	@1	@1%	@1	@1%	@1			
2018	PointNetVLAD [12]	Baseline	✓	[12], [160]	80.3	62.8	72.6	63.2	60.3	56.1	65.3	57.2	15	19.8
		Refine	✓	[12]	80.1	63.3	90.1	86.1	93.1	82.7	86.5	80.1		
	PointNetMax [12]	Baseline	✓	[12]	73.4		64.6		51.9		49.1			
		Refine	✓	[12]	73.9	54.2	79.3	62.2	75.1	60.2	69.5	58.6		
	PointNetSTD [12]	Baseline	✓	[12]	46.5		61.1		49.1		53.0			
		Refine	✓	[12]	46.5	31.9	57.0	45.7	59.8	44.3	53.0	44.5		
2019	PCAN [70]	Baseline	✓	[70], [156]	83.8	69.1	79.1	62.4	71.2	57.0	66.8	58.1	55	20.4
		Refine	✓	[70]	86.4	70.7	94.1	83.7	92.5	82.5	87.0	80.3		
	SeqLPD [242]			[242]	95.8	87.2						19	2.0	
	LPD-Net [5]	Baseline		[156], [160]	94.9	86.3	96.0	87.0	90.5	83.1	89.1	82.5	24	19.8
		Refine		[160]	94.9	86.6	98.9	94.4	96.4	90.8	94.4	90.8		
	2020	DAGC [13]	Baseline		[13]	87.5		83.5		75.7		71.2		
Refine				[13]	87.8	71.4	94.3	86.3	93.4	82.8	88.5	81.3		
DH3D [71]		✓	[69], [71]	84.3	73.3	81.5	64.4	72.1	57.9	68.4	60.1	36	18.9	
PIC-NET [172]				[157]	98.2									
SR-Net [153]		Baseline		[153]	94.6	86.8	94.3	86.8	89.2	80.2	83.5	77.3		
		Refine		[153]	95.3	88.5	98.5	93.5	93.6	86.8	90.8	85.9		
2021	PPT-Net [155]	Baseline	✓	[155]	98.1	93.5	97.5	90.1	93.3	84.1	90.0	84.6	22	13.1
		Refine	✓	[155]	98.4		99.7		99.5		95.3			
	SOE-Net [151]	Baseline	✓	[69]	93.4	84.2	91.1	80.0	87.0	75.9	83.8	77.2	59	19.4
		Refine	✓	[151]	96.4	89.3	97.7	91.8	95.9	90.2	92.6	89.0		
	MinkLoc3D [156]	Baseline	✓	[156]	98.5	94.8	99.7	97.2	99.3	96.7	96.7	94.0	21	1.1
		Refine	✓	[156], [160]	98.5	94.8	99.7	97.2	99.3	96.7	96.7	94.0		
	MinkLoc++ [157]	✓	[157]	99.1	96.7	99.5	96.5	98.5	95.3	95.5	91.8			
	NDT-Transformer [166]	✓	[161]	97.7	93.8							34		
	DiSCO [68]	✓	[68]	75.0	88.4							9		
	CORAL [18]		[18]	96.1	88.9							11		
	vLPD-Net [154]	✓	[154]	73.1	53.5									
	TransLoc3D [159]	Baseline		[159]	98.5	95.0	94.9		91.5		88.4			
Refine			[159]	98.5	95.0	99.8	97.5	99.7	97.3	97.4	94.8			
2022	SVT-Net [8]	Baseline		[8]	97.8	93.7	96.5	90.1	92.7	84.3	90.7	85.5	13	0.9
		Refine		[8]	98.4	94.7	99.9	97.0	99.5	95.2	97.2	94.4	13	0.9
	ASVT-Net [8]	Baseline		[8]	98.0	93.9	96.1	87.9	92.0	83.3	88.4	82.3	11	0.4
		Refine		[8]	98.3	94.6	99.6	97.5	98.9	95.0	97.0	94.5	11	0.4
	CSVT-Net [8]	Baseline		[8]	97.7	93.1	95.5	88.3	92.3	82.7	89.5	83.3	12	0.8
		Refine		[8]	98.6	94.8	99.8	96.6	98.7	96.2	97.3	94.3	12	0.8
	EPC-Net [69]	✓	[69]	94.7	86.2	96.5	88.2	88.6	80.2	84.9	78.1	33	4.7	
	EPC-Net-L [69]	✓	[69]	86.5	73.0	82.9	68.9	76.9	62.5	72.2	64.0	26	0.4	
	EPC-Net-L-D [69]	✓	[69]	92.2	80.3	87.2	74.9	80.0	66.8	75.5	67.0	26	0.4	
	HiTPR [165]		[165]	93.7	86.6	90.2	80.9	87.2	78.2	79.8	74.3	36	2.7	
	HiTPR-S8 [165]		[165]	93.6	86.6	85.6	75.8	75.0	63.1	71.3	64.5	36	2.7	
	HiTPR-F8 [165]		[165]	94.6	87.8	94.0	86.0	89.1	81.3	88.3	81.8			
	MinkLoc3D-I [161]	✓	[161]	98.1	93.6									
	MinkLoc3D-S [161]	✓	[161]	92.0	79.9									
	MinkLoc3D-SI [161]	✓	[161]	93.4	82.2							11		
	Retriever [14]		[14]	91.9		91.9			87.4		85.5			
	MinkLoc3Dv2 [160]	Baseline	✓	[160]	98.9	96.3	96.7	90.9	93.8	86.5	91.2	86.3		
		Refine	✓	[160]	99.1	96.9	99.7	99.0	99.4	98.3	99.1	97.6		

localization robustness by employing magnetic field sensors. Multi-robot systems can improve formation stability by emulating the cooperative behavior seen in bird flocks.

11.3 Advanced Sensors

Equipping robots with advanced sensors can enhance their navigation capabilities. We present several promising sensors as follows:

Solid-State LiDAR. Unlike mechanical LiDAR, solid-state LiDAR employs a micro-electro-mechanical system (MEMS), optical phased array (OPA), or flash technology for signal transmission and reception. It boasts a compact size, high resolution, fast scanning speed, and extended measurement range. It enables precise identification of buildings, pedestrians, vehicles, and traffic signs, effectively ensuring autonomous driving safety, supporting smart transportation data, and monitoring traffic accidents.

Event Camera. Instead of conventional fixed-frequency acquisition, event cameras exclusively generate an asyn-

chronous event stream when notable visual changes occur. They offer numerous benefits, including high time resolution, low latency, wide dynamic range, and low power consumption. Equipping vehicles with event cameras enhances obstacle avoidance in high-speed scenarios, enables navigation through scenes with abrupt light changes, and facilitates handling emergencies.

Millimeter Wave Radar. Millimeter-wave radar employs frequency-modulated continuous wave (FMCW) signals and mixers to measure speed, distance, and direction, providing cost-effectiveness, precise longitudinal ranging, accurate object detection, weather resistance, and high bandwidth. It will find wide applications in blind spot detection, object detection and tracking, parking assistance, and adaptive cruise control.

11.4 Significant Applications

As a new scientific and technological revolution unfolds, robot technology will spearhead advancements in several

critical fields shaping the fate of humanity:

Space Exploration. In inhospitable environments like the moon, robots will assume the role of humans, undertaking tasks such as terrain mapping, mineral identification, house construction, and 3D printing. They will aid human understanding of deep space and other planets.

Polar Research. Robots advance polar research by enhancing data collection capabilities. They collect data on glaciers, weather, and temperature, facilitating continuous environmental monitoring. High-resolution mapping of polar topography helps identify landform changes, glacier movement, and geological processes.

Underwater Robots. Underwater robots are advanced submersibles tailored for extreme underwater operations. The fiber optic gyroscope and Doppler log will greatly enhance localization performance, benefiting port construction and naval defense. Sonar detection technology will further improve task efficiency like underwater rescue and pipeline maintenance.

11.5 Approach Evaluations

A fair and thorough evaluation is crucial for adapting robot products, algorithms, and scenarios. Here are three pivotal considerations for future algorithm evaluation.

Scalability and Efficiency. The growing affordability and accessibility of LiDAR sensors have spurred the demand for large-scale place recognition. This necessitates the development of scalable algorithms for handling large-scale point clouds and the design of efficient algorithms for the real-time processing of point cloud data on resource-constrained platforms.

Long-term Place Recognition. Long-term place recognition refers to the ability of a system to identify places over extended periods, despite appearance and weather variations. It is a crucial capability for autonomous navigation. Designing algorithms that can handle seasons, weather, appearances, and dynamic objects, will drive significant advancements in this field.

Standardized Datasets. A good dataset should possess sufficient size, high-quality data, reliable ground truth, annotations or labels, ethical considerations, normalized form, and clear instructions. Creating diverse data encompassing various sensor modalities, environmental conditions, and weather changes is also highly valuable.

11.6 Learning-based Improvement

Learning-based LPR methods have demonstrated impressive results, and we outline promising directions to improve their performance as follows:

Network Design. Transformer-based networks [155], [165], [166], [169], [170] are computationally expensive for large-scale datasets. To address this, techniques like model compression and efficient attention mechanisms can be used to reduce computational requirements.

Loss Function. The lazy quadruplet loss [12], [13], [165], [166], [172] is prone to overfitting with limited training data. Regularization techniques like weight decay, dropout, or batch normalization may enhance generalization performance.

Training Strategy. End-to-end networks [9], [12], [13], [68], [151], [152], [162], [168], [174] commonly demand large amounts of labeled data for training. Transfer learning and semi-supervised learning may enhance training efficiency.

12 CONCLUSIONS

This paper is the first comprehensive survey specifically dedicated to LPR research to the best of our knowledge. It provides extensive discussions on the background of place recognition, highlighting the primary concerns in current research. We conduct a comprehensive method classification and performance comparison, elucidating their architectures, strengths, and weaknesses. Furthermore, we summarize commonly employed datasets, evaluation metrics, and promising future directions.

REFERENCES

- [1] A. Torii, J. Sivic, M. Okutomi, and T. Pajdla, "Visual place recognition with repetitive structures," *IEEE Transactions on Pattern Analysis and Machine Intelligence*, vol. 37, no. 11, pp. 2346–2359, 2015.
- [2] S. Lowry and M. J. Milford, "Supervised and unsupervised linear learning techniques for visual place recognition in changing environments," *IEEE Transactions on Robotics*, vol. 32, no. 3, pp. 600–613, 2016.
- [3] D. L. Rizzini, "Place recognition of 3d landmarks based on geometric relations," in *2017 IEEE/RSJ International Conference on Intelligent Robots and Systems (IROS)*. IEEE, 2017, pp. 648–654.
- [4] G. Kim and A. Kim, "Scan context: Egocentric spatial descriptor for place recognition within 3d point cloud map," in *2018 IEEE/RSJ International Conference on Intelligent Robots and Systems (IROS)*. IEEE, 2018, pp. 4802–4809.
- [5] Z. Liu, S. Zhou, C. Suo, P. Yin, W. Chen, H. Wang, H. Li, and Y.-H. Liu, "Lpd-net: 3d point cloud learning for large-scale place recognition and environment analysis," in *Proceedings of the IEEE/CVF International Conference on Computer Vision*, 2019, pp. 2831–2840.
- [6] P. Yin, F. Wang, A. Egorov, J. Hou, J. Zhang, and H. Choset, "Seqspherevlad: Sequence matching enhanced orientation-invariant place recognition," in *2020 IEEE/RSJ International Conference on Intelligent Robots and Systems (IROS)*, 2020, pp. 5024–5029.
- [7] G. Kim, S. Choi, and A. Kim, "Scan context++: Structural place recognition robust to rotation and lateral variations in urban environments," *IEEE Transactions on Robotics*, 2021.
- [8] Z. Fan, Z. Song, H. Liu, Z. Lu, J. He, and X. Du, "Svt-net: Super light-weight sparse voxel transformer for large scale place recognition," in *Proceedings of the AAAI Conference on Artificial Intelligence*, vol. 36, no. 1, 2022, pp. 551–560.
- [9] G. Kim, B. Park, and A. Kim, "1-day learning, 1-year localization: Long-term lidar localization using scan context image," *IEEE Robotics and Automation Letters*, vol. 4, no. 2, pp. 1948–1955, 2019.
- [10] H. Dong, X. Chen, and C. Stachniss, "Online range image-based pole extractor for long-term lidar localization in urban environments," in *2021 European Conference on Mobile Robots (ECMR)*. IEEE, 2021, pp. 1–6.
- [11] F. Cao, H. Wu, and C. Wu, "An end-to-end localizer for long-term topological localization in large-scale changing environments," *IEEE Transactions on Industrial Electronics*, pp. 1–10, 2022.
- [12] M. A. Uy and G. H. Lee, "Pointnetvlad: Deep point cloud based retrieval for large-scale place recognition," in *Proceedings of the IEEE conference on computer vision and pattern recognition*, 2018, pp. 4470–4479.
- [13] Q. Sun, H. Liu, J. He, Z. Fan, and X. Du, "Dagc: Employing dual attention and graph convolution for point cloud based place recognition," in *Proceedings of the 2020 International Conference on Multimedia Retrieval*, 2020, pp. 224–232.
- [14] L. Wiesmann, R. Marcuzzi, C. Stachniss, and J. Behley, "Retriever: Point cloud retrieval in compressed 3d maps," in *2022 International Conference on Robotics and Automation (ICRA)*, 2022, pp. 10 925–10 932.

- [15] B. Steder, M. Ruhnke, S. Grzonka, and W. Burgard, "Place recognition in 3d scans using a combination of bag of words and point feature based relative pose estimation," in *2011 IEEE/RSJ International Conference on Intelligent Robots and Systems*, 2011, pp. 1249–1255.
- [16] A. Torii, R. Arandjelović, J. Sivic, M. Okutomi, and T. Pajdla, "24/7 place recognition by view synthesis," *IEEE Transactions on Pattern Analysis and Machine Intelligence*, vol. 40, no. 2, pp. 257–271, 2018.
- [17] A. Khaliq, S. Ehsan, Z. Chen, M. Milford, and K. McDonald-Maier, "A holistic visual place recognition approach using lightweight cnns for significant viewpoint and appearance changes," *IEEE transactions on robotics*, vol. 36, no. 2, pp. 561–569, 2019.
- [18] Y. Pan, X. Xu, W. Li, Y. Cui, Y. Wang, and R. Xiong, "Coral: Colored structural representation for bi-modal place recognition," in *2021 IEEE/RSJ International Conference on Intelligent Robots and Systems (IROS)*, 2021, pp. 2084–2091.
- [19] H. Yin, Y. Wang, X. Ding, L. Tang, S. Huang, and R. Xiong, "3d lidar-based global localization using siamese neural network," *IEEE Transactions on Intelligent Transportation Systems*, vol. 21, no. 4, pp. 1380–1392, 2020.
- [20] S.-Y. An and J. Kim, "Extracting statistical signatures of geometry and structure in 2d occupancy grid maps for global localization," *IEEE Robotics and Automation Letters*, vol. 7, no. 2, pp. 4291–4298, 2022.
- [21] Y. Li, Y. Cai, Z. Li, S. Feng, H. Wang, and M. A. Sotelo, "Map-based localization for intelligent vehicles from bi-sensor data fusion," *Expert Systems with Applications*, vol. 203, p. 117586, 2022.
- [22] T. Schmiedel, E. Einhorn, and H.-M. Gross, "Iron: A fast interest point descriptor for robust ndt-map matching and its application to robot localization," in *2015 IEEE/RSJ International Conference on Intelligent Robots and Systems (IROS)*. IEEE, 2015, pp. 3144–3151.
- [23] H. Song, W. Choi, and H. Kim, "Robust vision-based relative-localization approach using an rgb-depth camera and lidar sensor fusion," *IEEE Transactions on Industrial Electronics*, vol. 63, no. 6, pp. 3725–3736, 2016.
- [24] A. Y. Hata and D. F. Wolf, "Feature detection for vehicle localization in urban environments using a multilayer lidar," *IEEE Transactions on Intelligent Transportation Systems*, vol. 17, no. 2, pp. 420–429, 2016.
- [25] G. Elbaz, T. Avraham, and A. Fischer, "3d point cloud registration for localization using a deep neural network auto-encoder," in *Proceedings of the IEEE conference on computer vision and pattern recognition*, 2017, pp. 4631–4640.
- [26] W. Lu, Y. Zhou, G. Wan, S. Hou, and S. Song, "L3-net: Towards learning based lidar localization for autonomous driving," in *Proceedings of the IEEE/CVF Conference on Computer Vision and Pattern Recognition*, 2019, pp. 6389–6398.
- [27] H. Wang, C. Wang, and L. Xie, "Lightweight 3-d localization and mapping for solid-state lidar," *IEEE Robotics and Automation Letters*, vol. 6, no. 2, pp. 1801–1807, 2021.
- [28] D. Schleicher, L. M. Bergasa, M. Ocaña, R. Barea, and M. E. López, "Real-time hierarchical outdoor slam based on stereovision and gps fusion," *IEEE Transactions on Intelligent Transportation Systems*, vol. 10, no. 3, pp. 440–452, 2009.
- [29] O. Vysotska, T. Naseer, L. Spinello, W. Burgard, and C. Stachniss, "Efficient and effective matching of image sequences under substantial appearance changes exploiting gps priors," in *2015 IEEE International Conference on Robotics and Automation (ICRA)*, 2015, pp. 2774–2779.
- [30] K. Pargiela and A. Rzonca, "Determining optimal photogrammetric adjustment of images obtained from a fixed-wing uav," *The Photogrammetric Record*, vol. 36, no. 175, pp. 285–302, 2021.
- [31] Y. Yang and G. Huang, "Observability analysis of aided ins with heterogeneous features of points, lines, and planes," *IEEE Transactions on Robotics*, vol. 35, no. 6, pp. 1399–1418, 2019.
- [32] K.-W. Chiang, G.-J. Tsai, H.-J. Chu, and N. El-Sheimy, "Performance enhancement of ins/gnss/refreshed-slam integration for acceptable lane-level navigation accuracy," *IEEE Transactions on Vehicular Technology*, vol. 69, no. 3, pp. 2463–2476, 2020.
- [33] J. J. Morales and Z. M. Kassas, "Tightly coupled inertial navigation system with signals of opportunity aiding," *IEEE Transactions on Aerospace and Electronic Systems*, vol. 57, no. 3, pp. 1930–1948, 2021.
- [34] M. Bagherbandi, A. Jouybari, F. Nilfouroushan, and J. Ågren, "Deflection of vertical effect on direct georeferencing in aerial mobile mapping systems: A case study in sweden," *The Photogrammetric Record*, vol. 37, no. 179, pp. 285–305, 2022.
- [35] G. P. C. Júnior, A. M. C. Rezende, V. R. F. Miranda, R. Fernandes, H. Azpúrua, A. A. Neto, G. Pessin, and G. M. Freitas, "Ekf-loam: An adaptive fusion of lidar slam with wheel odometry and inertial data for confined spaces with few geometric features," *IEEE Transactions on Automation Science and Engineering*, vol. 19, no. 3, pp. 1458–1471, 2022.
- [36] S. Lowry, N. Sünderhauf, P. Newman, J. J. Leonard, D. Cox, P. Corke, and M. J. Milford, "Visual place recognition: A survey," *IEEE Transactions on Robotics*, vol. 32, no. 1, pp. 1–19, 2016.
- [37] R. Power, M. Zaffar, B. Ferrarini, M. Milford, K. McDonald-Maier, and S. Ehsan, "A benchmark comparison of visual place recognition techniques for resource-constrained embedded platforms," *arXiv preprint arXiv:2109.11002*, 2021.
- [38] J. Peltomäki, F. Aljani, J. Puura, H. Huttunen, E. Rahtu, and J.-K. Kämäräinen, "Evaluation of long-term lidar place recognition," in *2021 IEEE/RSJ International Conference on Intelligent Robots and Systems (IROS)*, 2021, pp. 4487–4492.
- [39] K. A. Tsintotas, L. Bampis, and A. Gasteratos, "The revisiting problem in simultaneous localization and mapping: A survey on visual loop closure detection," *IEEE Transactions on Intelligent Transportation Systems*, vol. 23, no. 11, pp. 19929–19953, 2022.
- [40] X. Zhang, L. Wang, and Y. Su, "Visual place recognition: A survey from deep learning perspective," *Pattern Recognition*, vol. 113, p. 107760, 2021.
- [41] J. Li, W. Xu, P. Shi, Y. Zhang, and Q. Hu, "Lknif: Locally normalized image for rotation invariant multimodal feature matching," *IEEE Transactions on Geoscience and Remote Sensing*, vol. 60, pp. 1–14, 2022.
- [42] J. Wu and J. M. Rehg, "Centrist: A visual descriptor for scene categorization," *IEEE Transactions on Pattern Analysis and Machine Intelligence*, vol. 33, no. 8, pp. 1489–1501, 2011.
- [43] R. Arandjelovic, P. Gronat, A. Torii, T. Pajdla, and J. Sivic, "Netvlad: Cnn architecture for weakly supervised place recognition," in *Proceedings of the IEEE conference on computer vision and pattern recognition*, 2016, pp. 5297–5307.
- [44] R. Wang, Y. Shen, W. Zuo, S. Zhou, and N. Zheng, "Transvpr: Transformer-based place recognition with multi-level attention aggregation," in *Proceedings of the IEEE/CVF Conference on Computer Vision and Pattern Recognition*, 2022, pp. 13648–13657.
- [45] P. Shi, Q. Ye, and L. Zeng, "A novel indoor structure extraction based on dense point cloud," *ISPRS International Journal of Geo-Information*, vol. 9, no. 11, p. 660, 2020.
- [46] H. Wang, C. Wang, and L. Xie, "Intensity scan context: Coding intensity and geometry relations for loop closure detection," in *2020 IEEE International Conference on Robotics and Automation (ICRA)*. IEEE, 2020, pp. 2095–2101.
- [47] Y. Wang, Z. Sun, C.-Z. Xu, S. E. Sarma, J. Yang, and H. Kong, "Lidar iris for loop-closure detection," in *2020 IEEE/RSJ International Conference on Intelligent Robots and Systems (IROS)*. IEEE, 2020, pp. 5769–5775.
- [48] T. Röhling, J. Mack, and D. Schulz, "A fast histogram-based similarity measure for detecting loop closures in 3-d lidar data," in *2015 IEEE/RSJ International Conference on Intelligent Robots and Systems (IROS)*. IEEE, 2015, pp. 736–741.
- [49] L. Luo, S.-Y. Cao, Z. Sheng, and H.-L. Shen, "Lidar-based global localization using histogram of orientations of principal normals," *IEEE Transactions on Intelligent Vehicles*, vol. 7, no. 3, pp. 771–782, 2022.
- [50] L. Schaupp, M. Bürki, R. Dubé, R. Siegwart, and C. Cadena, "Oreos: Oriented recognition of 3d point clouds in outdoor scenarios," in *2019 IEEE/RSJ International Conference on Intelligent Robots and Systems (IROS)*. IEEE, 2019, pp. 3255–3261.
- [51] X. Kong, X. Yang, G. Zhai, X. Zhao, X. Zeng, M. Wang, Y. Liu, W. Li, and F. Wen, "Semantic graph based place recognition for 3d point clouds," in *2020 IEEE/RSJ International Conference on Intelligent Robots and Systems (IROS)*. IEEE, 2020, pp. 8216–8223.
- [52] Y. Zhu, Y. Ma, L. Chen, C. Liu, M. Ye, and L. Li, "Gosmatch: Graph-of-semantics matching for detecting loop closures in 3d lidar data," in *2020 IEEE/RSJ International Conference on Intelligent Robots and Systems (IROS)*. IEEE, 2020, pp. 5151–5157.
- [53] L. Li, X. Kong, X. Zhao, W. Li, F. Wen, H. Zhang, and Y. Liu, "Saloom: Semantic-aided lidar slam with loop closure," in *2021 IEEE International Conference on Robotics and Automation (ICRA)*. IEEE, 2021, pp. 7627–7634.

- [54] L. Luo, S.-Y. Cao, B. Han, H.-L. Shen, and J. Li, "Bvmatch: Lidar-based place recognition using bird's-eye view images," *IEEE Robotics and Automation Letters*, vol. 6, no. 3, pp. 6076–6083, 2021.
- [55] T. Shan, B. Englot, D. Meyers, W. Wang, C. Ratti, and D. Rus, "Lio-sam: Tightly-coupled lidar inertial odometry via smoothing and mapping," in *2020 IEEE/RSJ International Conference on Intelligent Robots and Systems (IROS)*, 2020, pp. 5135–5142.
- [56] Y. Zhang, "Lilo: A novel lidar-imu slam system with loop optimization," *IEEE Transactions on Aerospace and Electronic Systems*, 2021.
- [57] P. Yin, F. Wang, A. Egorov, J. Hou, Z. Jia, and J. Han, "Fast sequence-matching enhanced viewpoint-invariant 3-d place recognition," *IEEE Transactions on Industrial Electronics*, vol. 69, no. 2, pp. 2127–2135, 2022.
- [58] T. Shan and B. Englot, "Lego-loam: Lightweight and ground-optimized lidar odometry and mapping on variable terrain," in *2018 IEEE/RSJ International Conference on Intelligent Robots and Systems (IROS)*. IEEE, 2018, pp. 4758–4765.
- [59] P. Dellenbach, J.-E. Deschaud, B. Jacquet, and F. Goulette, "Ct-icp: Real-time elastic lidar odometry with loop closure," in *2022 International Conference on Robotics and Automation (ICRA)*, 2022, pp. 5580–5586.
- [60] J. Li, P. Shi, Q. Hu, and Y. Zhang, "Qgore: Quadratic-time guaranteed outlier removal for point cloud registration," *IEEE Transactions on Pattern Analysis and Machine Intelligence*, 2023.
- [61] M. Bosse and R. Zlot, "Place recognition using keypoint voting in large 3d lidar datasets," in *2013 IEEE International Conference on Robotics and Automation*, 2013, pp. 2677–2684.
- [62] N. Muhammad and S. Lacroix, "Loop closure detection using small-sized signatures from 3d lidar data," in *2011 IEEE International Symposium on Safety, Security, and Rescue Robotics*. IEEE, 2011, pp. 333–338.
- [63] J. Guo, P. V. Borges, C. Park, and A. Gawel, "Local descriptor for robust place recognition using lidar intensity," *IEEE Robotics and Automation Letters*, vol. 4, no. 2, pp. 1470–1477, 2019.
- [64] K. P. Cop, P. V. Borges, and R. Dubé, "Delight: An efficient descriptor for global localisation using lidar intensities," in *2018 IEEE International Conference on Robotics and Automation (ICRA)*. IEEE, 2018, pp. 3653–3660.
- [65] H. Xiang, W. Shi, W. Fan, P. Chen, S. Bao, and M. Nie, "Fastlcd: A fast and compact loop closure detection approach using 3d point cloud for indoor mobile mapping," *International Journal of Applied Earth Observation and Geoinformation*, vol. 102, p. 102430, 2021.
- [66] S. Ratz, M. Dymczyk, R. Siegwart, and R. Dubé, "Oneshot global localization: Instant lidar-visual pose estimation," in *2020 IEEE International conference on Robotics and Automation (ICRA)*. IEEE, 2020, pp. 5415–5421.
- [67] D. Xu, J. Liu, J. Hyypää, Y. Liang, and W. Tao, "A heterogeneous 3d map-based place recognition solution using virtual lidar and a polar grid height coding image descriptor," *ISPRS Journal of Photogrammetry and Remote Sensing*, vol. 183, pp. 1–18, 2022.
- [68] X. Xu, H. Yin, Z. Chen, Y. Li, Y. Wang, and R. Xiong, "Disco: Differentiable scan context with orientation," *IEEE Robotics and Automation Letters*, vol. 6, no. 2, pp. 2791–2798, 2021.
- [69] L. Hui, M. Cheng, J. Xie, J. Yang, and M.-M. Cheng, "Efficient 3d point cloud feature learning for large-scale place recognition," *IEEE Transactions on Image Processing*, vol. 31, pp. 1258–1270, 2022.
- [70] W. Zhang and C. Xiao, "Pcan: 3d attention map learning using contextual information for point cloud based retrieval," in *Proceedings of the IEEE/CVF Conference on Computer Vision and Pattern Recognition*, 2019, pp. 12 436–12 445.
- [71] J. Du, R. Wang, and D. Cremers, "Dh3d: Deep hierarchical 3d descriptors for robust large-scale 6dof relocalization," in *European Conference on Computer Vision*. Springer, 2020, pp. 744–762.
- [72] X. Chen, T. Lbe, A. Milioto, T. Rhling, and C. Stachniss, "Overlapnet: Loop closing for lidar-based slam," in *Robotics: Science and Systems 2020*, 2020.
- [73] L. Li, X. Kong, X. Zhao, T. Huang, W. Li, F. Wen, H. Zhang, and Y. Liu, "Ssc: Semantic scan context for large-scale place recognition," in *2021 IEEE/RSJ International Conference on Intelligent Robots and Systems (IROS)*. IEEE, 2021, pp. 2092–2099.
- [74] R. Dubé, D. Dugas, E. Stumm, J. Nieto, R. Siegwart, and C. Cadena, "Segmatch: Segment based place recognition in 3d point clouds," in *2017 IEEE International Conference on Robotics and Automation (ICRA)*, 2017, pp. 5266–5272.
- [75] D. Xu, J. Liu, Y. Liang, X. Lv, and J. Hyypää, "A lidar-based single-shot global localization solution using a cross-section shape context descriptor," *ISPRS Journal of Photogrammetry and Remote Sensing*, vol. 189, pp. 272–288, 2022.
- [76] X. Chen, A. Milioto, E. Palazzolo, P. Giguere, J. Behley, and C. Stachniss, "Suma++: Efficient lidar-based semantic slam," in *2019 IEEE/RSJ International Conference on Intelligent Robots and Systems (IROS)*. IEEE, 2019, pp. 4530–4537.
- [77] X. Chen, I. Vizzo, T. Läbe, J. Behley, and C. Stachniss, "Range image-based lidar localization for autonomous vehicles," in *2021 IEEE International Conference on Robotics and Automation (ICRA)*, 2021, pp. 5802–5808.
- [78] H. Wang, C. Wang, C.-L. Chen, and L. Xie, "F-loam : Fast lidar odometry and mapping," in *2021 IEEE/RSJ International Conference on Intelligent Robots and Systems (IROS)*, 2021, pp. 4390–4396.
- [79] Y. Pan, P. Xiao, Y. He, Z. Shao, and Z. Li, "Mulls: Versatile lidar slam via multi-metric linear least square," in *2021 IEEE International Conference on Robotics and Automation (ICRA)*. IEEE, 2021, pp. 11 633–11 640.
- [80] K. Żywanowski, A. Banaszczyk, and M. R. Nowicki, "Comparison of camera-based and 3d lidar-based place recognition across weather conditions," in *2020 16th International Conference on Control, Automation, Robotics and Vision (ICARCV)*, 2020, pp. 886–891.
- [81] P. Shi, Q. Ye, Z. Shaoming, and D. Haifeng, "Localization initialization for multi-beam lidar considering indoor scene feature," *Acta Geodaetica et Cartographica Sinica*, vol. 50, pp. 1594–1604, 2021.
- [82] P. Shi, J. Li, and Y. Zhang, "Lidar localization at 100 fps: A map-aided and template descriptor-based global method," *International Journal of Applied Earth Observation and Geoinformation*, vol. 120, p. 103336, 2023.
- [83] J. Zhang and S. Singh, "Low-drift and real-time lidar odometry and mapping," *Autonomous Robots*, vol. 41, no. 2, pp. 401–416, 2017.
- [84] J. Lin and F. Zhang, "A fast, complete, point cloud based loop closure for lidar odometry and mapping," *arXiv preprint arXiv:1909.11811*, 2019.
- [85] D. Wilson, X. Zhang, W. Sultani, and S. Wshah, "Visual and object geo-localization: A comprehensive survey," *arXiv preprint arXiv:2112.15202*, 2021.
- [86] E. Mahdi and H. Xinming, "A survey on visual map localization using lidars and cameras," *arXiv preprint arXiv:2208.03376*, 2022.
- [87] F. Chen, X. Wang, Y. Zhao, S. Lv, and X. Niu, "Visual object tracking: A survey," *Computer Vision and Image Understanding*, vol. 222, p. 103508, 2022.
- [88] S. M. Marvasti-Zadeh, L. Cheng, H. Ghanei-Yakhdan, and S. Kasaei, "Deep learning for visual tracking: A comprehensive survey," *IEEE Transactions on Intelligent Transportation Systems*, 2021.
- [89] I. A. Kazerouni, L. Fitzgerald, G. Dooly, and D. Toal, "A survey of state-of-the-art on visual slam," *Expert Systems with Applications*, p. 117734, 2022.
- [90] S. Zhang, S. Zhao, D. An, J. Liu, H. Wang, Y. Feng, D. Li, and R. Zhao, "Visual slam for underwater vehicles: A survey," *Computer Science Review*, vol. 46, p. 100510, 2022.
- [91] K. Huang, S. Zhang, J. Zhang, and D. Tao, "Event-based simultaneous localization and mapping: A comprehensive survey," *arXiv preprint arXiv:2304.09793*, 2023.
- [92] C. Cadena, L. Carlone, H. Carrillo, Y. Latif, D. Scaramuzza, J. Neira, I. Reid, and J. J. Leonard, "Past, present, and future of simultaneous localization and mapping: Toward the robust-perception age," *IEEE Transactions on robotics*, vol. 32, no. 6, pp. 1309–1332, 2016.
- [93] P. Yin, S. Zhao, I. Cisneros, A. Abuduweili, G. Huang, M. Milford, C. Liu, H. Choset, and S. Scherer, "General place recognition survey: Towards the real-world autonomy age," *arXiv preprint arXiv:2209.04497*, 2022.
- [94] H. Yin, X. Xu, S. Lu, X. Chen, R. Xiong, S. Shen, C. Stachniss, and Y. Wang, "A survey on global lidar localization: Challenges, advances and open problems," *arXiv preprint arXiv:2302.07433*, 2023.
- [95] A. E. Johnson and M. Hebert, "Using spin images for efficient object recognition in cluttered 3d scenes," *IEEE Transactions on pattern analysis and machine intelligence*, vol. 21, no. 5, pp. 433–449, 1999.
- [96] A. Frome, D. Huber, R. Kolluri, T. Bülow, and J. Malik, "Recognizing objects in range data using regional point descriptors," in

- European conference on computer vision.* Springer, 2004, pp. 224–237.
- [97] R. B. Rusu, N. Blodow, Z. C. Marton, and M. Beetz, “Aligning point cloud views using persistent feature histograms,” in *2008 IEEE/RSJ international conference on intelligent robots and systems*. IEEE, 2008, pp. 3384–3391.
- [98] R. B. Rusu, N. Blodow, and M. Beetz, “Fast point feature histograms (fpfh) for 3d registration,” in *2009 IEEE international conference on robotics and automation*. IEEE, 2009, pp. 3212–3217.
- [99] T. Cieslewski, E. Stumm, A. Gawel, M. Bosse, S. Lynen, and R. Siegwart, “Point cloud descriptors for place recognition using sparse visual information,” in *2016 IEEE International Conference on Robotics and Automation (ICRA)*. IEEE, 2016, pp. 4830–4836.
- [100] H. Zhao, M. Tang, and H. Ding, “Hopppf: A novel local surface descriptor for 3d object recognition,” *Pattern Recognition*, vol. 103, p. 107272, 2020.
- [101] F. Tombari, S. Salti, and L. Di Stefano, “Unique shape context for 3d data description,” in *Proceedings of the ACM workshop on 3D object retrieval*, 2010, pp. 57–62.
- [102] Y. Guo, F. Sohel, M. Bennamoun, M. Lu, and J. Wan, “Rotational projection statistics for 3d local surface description and object recognition,” *International journal of computer vision*, vol. 105, no. 1, pp. 63–86, 2013.
- [103] S. Salti, F. Tombari, and L. Di Stefano, “Shot: Unique signatures of histograms for surface and texture description,” *Computer Vision and Image Understanding*, vol. 125, pp. 251–264, 2014.
- [104] J. Yang, Q. Zhang, Y. Xiao, and Z. Cao, “Toldi: An effective and robust approach for 3d local shape description,” *Pattern Recognition*, vol. 65, pp. 175–187, 2017.
- [105] T. Sun, G. Liu, S. Liu, F. Meng, L. Zeng, and R. Li, “An efficient and compact 3d local descriptor based on the weighted height image,” *Information Sciences*, vol. 520, pp. 209–231, 2020.
- [106] B. Steder, G. Grisetti, and W. Burgard, “Robust place recognition for 3d range data based on point features,” in *2010 IEEE International Conference on Robotics and Automation*. IEEE, 2010, pp. 1400–1405.
- [107] Y. Zhuang, N. Jiang, H. Hu, and F. Yan, “3-d-laser-based scene measurement and place recognition for mobile robots in dynamic indoor environments,” *IEEE Transactions on Instrumentation and Measurement*, vol. 62, no. 2, pp. 438–450, 2013.
- [108] F. Cao, Y. Zhuang, H. Zhang, and W. Wang, “Robust place recognition and loop closing in laser-based slam for ugvs in urban environments,” *IEEE Sensors Journal*, vol. 18, no. 10, pp. 4242–4252, 2018.
- [109] T. Shan, B. Englot, F. Duarte, C. Ratti, and D. Rus, “Robust place recognition using an imaging lidar,” in *2021 IEEE International Conference on Robotics and Automation (ICRA)*, 2021, pp. 5469–5475.
- [110] Z. Wu, S. Song, A. Khosla, F. Yu, L. Zhang, X. Tang, and J. Xiao, “3d shapenets: A deep representation for volumetric shapes,” in *2015 IEEE Conference on Computer Vision and Pattern Recognition (CVPR)*, 2015, pp. 1912–1920.
- [111] C. R. Qi, H. Su, M. Nießner, A. Dai, M. Yan, and L. J. Guibas, “Volumetric and multi-view cnns for object classification on 3d data,” in *Proceedings of the IEEE conference on computer vision and pattern recognition*, 2016, pp. 5648–5656.
- [112] A. Zeng, S. Song, M. Nießner, M. Fisher, J. Xiao, and T. Funkhouser, “3dmatch: Learning local geometric descriptors from rgb-d reconstructions,” in *2017 IEEE Conference on Computer Vision and Pattern Recognition (CVPR)*, 2017, pp. 199–208.
- [113] C. Choy, J. Park, and V. Koltun, “Fully convolutional geometric features,” in *2019 IEEE/CVF International Conference on Computer Vision (ICCV)*, 2019, pp. 8957–8965.
- [114] Z. Gojcic, C. Zhou, J. D. Wegner, and A. Wieser, “The perfect match: 3d point cloud matching with smoothed densities,” in *2019 IEEE/CVF Conference on Computer Vision and Pattern Recognition (CVPR)*, 2019, pp. 5540–5549.
- [115] S. Ao, Q. Hu, B. Yang, A. Markham, and Y. Guo, “Spinnet: Learning a general surface descriptor for 3d point cloud registration,” in *Proceedings of the IEEE/CVF conference on computer vision and pattern recognition*, 2021, pp. 11 753–11 762.
- [116] S. Ao, Y. Guo, Q. Hu, B. Yang, A. Markham, and Z. Chen, “You only train once: Learning general and distinctive 3d local descriptors,” *IEEE Transactions on Pattern Analysis and Machine Intelligence*, vol. 45, no. 3, pp. 3949–3967, 2023.
- [117] C. R. Qi, H. Su, K. Mo, and L. J. Guibas, “Pointnet: Deep learning on point sets for 3d classification and segmentation,” in *Proceedings of the IEEE conference on computer vision and pattern recognition*, 2017, pp. 652–660.
- [118] C. R. Qi, L. Yi, H. Su, and L. J. Guibas, “Pointnet++: Deep hierarchical feature learning on point sets in a metric space,” *Advances in neural information processing systems*, vol. 30, 2017.
- [119] M. Khoury, Q.-Y. Zhou, and V. Koltun, “Learning compact geometric features,” in *Proceedings of the IEEE international conference on computer vision*, 2017, pp. 153–161.
- [120] H. Deng, T. Birdal, and S. Ilic, “Ppfnet: Global context aware local features for robust 3d point matching,” in *2018 IEEE/CVF Conference on Computer Vision and Pattern Recognition*, 2018, pp. 195–205.
- [121] —, “Ppf-foldnet: Unsupervised learning of rotation invariant 3d local descriptors,” in *Proceedings of the European Conference on Computer Vision (ECCV)*, 2018, pp. 602–618.
- [122] W. Lu, G. Wan, Y. Zhou, X. Fu, P. Yuan, and S. Song, “Deepvcv: An end-to-end deep neural network for point cloud registration,” in *Proceedings of the IEEE/CVF International Conference on Computer Vision*, 2019, pp. 12–21.
- [123] H. Deng, T. Birdal, and S. Ilic, “3d local features for direct pairwise registration,” in *Proceedings of the IEEE/CVF Conference on Computer Vision and Pattern Recognition*, 2019, pp. 3244–3253.
- [124] X. Bai, Z. Luo, L. Zhou, H. Fu, L. Quan, and C.-L. Tai, “D3feat: Joint learning of dense detection and description of 3d local features,” in *Proceedings of the IEEE/CVF conference on computer vision and pattern recognition*, 2020, pp. 6359–6367.
- [125] Y. Zhou, Y. Wang, F. Poiesi, Q. Qin, and Y. Wan, “Loop closure detection using local 3d deep descriptors,” *IEEE Robotics and Automation Letters*, vol. 7, no. 3, pp. 6335–6342, 2022.
- [126] F. Poiesi and D. Boscaini, “Learning general and distinctive 3d local deep descriptors for point cloud registration,” *IEEE Transactions on Pattern Analysis and Machine Intelligence*, vol. 45, no. 3, pp. 3979–3985, 2022.
- [127] M. Marcon, R. Spezialetti, S. Salti, L. Silva, and L. D. Stefano, “Unsupervised learning of local equivariant descriptors for point clouds,” *IEEE Transactions on Pattern Analysis and Machine Intelligence*, vol. 44, no. 12, pp. 9687–9702, 2022.
- [128] L. Zhou, S. Zhu, Z. Luo, T. Shen, R. Zhang, M. Zhen, T. Fang, and L. Quan, “Learning and matching multi-view descriptors for registration of point clouds,” in *Proceedings of the European Conference on Computer Vision (ECCV)*, 2018, pp. 505–522.
- [129] L. Li, S. Zhu, H. Fu, P. Tan, and C.-L. Tai, “End-to-end learning local multi-view descriptors for 3d point clouds,” in *2020 IEEE/CVF Conference on Computer Vision and Pattern Recognition (CVPR)*, 2020, pp. 1916–1925.
- [130] Z. Gojcic, C. Zhou, J. D. Wegner, L. J. Guibas, and T. Birdal, “Learning multiview 3d point cloud registration,” in *2020 IEEE/CVF Conference on Computer Vision and Pattern Recognition (CVPR)*, 2020, pp. 1756–1766.
- [131] H. Xiang, X. Zhu, W. Shi, W. Fan, P. Chen, and S. Bao, “Delightlcd: A deep and lightweight network for loop closure detection in lidar slam,” *IEEE Sensors Journal*, vol. 22, no. 21, pp. 20 761–20 772, 2022.
- [132] B. Steder, G. Grisetti, M. Van Loock, and W. Burgard, “Robust on-line model-based object detection from range images,” in *2009 IEEE/RSJ International Conference on Intelligent Robots and Systems*. IEEE, 2009, pp. 4739–4744.
- [133] J. Li, Q. Hu, and M. Ai, “Rift: Multi-modal image matching based on radiation-variation insensitive feature transform,” *IEEE Transactions on Image Processing*, vol. 29, pp. 3296–3310, 2020.
- [134] E. Rosten and T. Drummond, “Machine learning for high-speed corner detection,” in *Computer Vision—ECCV 2006: 9th European Conference on Computer Vision, Graz, Austria, May 7–13, 2006. Proceedings, Part I 9*. Springer, 2006, pp. 430–443.
- [135] Y. Guo, M. Bennamoun, F. Sohel, M. Lu, and J. Wan, “3d object recognition in cluttered scenes with local surface features: A survey,” *IEEE Transactions on Pattern Analysis and Machine Intelligence*, vol. 36, no. 11, pp. 2270–2287, 2014.
- [136] J. Yang, S. Quan, P. Wang, and Y. Zhang, “Evaluating local geometric feature representations for 3d rigid data matching,” *IEEE Transactions on Image Processing*, vol. 29, pp. 2522–2535, 2020.
- [137] Y. Guo, M. Bennamoun, F. Sohel, M. Lu, J. Wan, and N. M. Kwok, “A comprehensive performance evaluation of 3d local feature descriptors,” *International Journal of Computer Vision*, vol. 116, pp. 66–89, 2016.
- [138] Y. Zhong, “Intrinsic shape signatures: A shape descriptor for 3d object recognition,” in *2009 IEEE 12th international conference on*

- computer vision workshops, ICCV Workshops*. IEEE, 2009, pp. 689–696.
- [139] X. Shi, Z. Chai, Y. Zhou, J. Wu, and Z. Xiong, “Global place recognition using an improved scan context for lidar-based localization system,” in *2021 IEEE/ASME International Conference on Advanced Intelligent Mechatronics (AIM)*, 2021, pp. 498–503.
- [140] X. Cai and W. Yin, “Weighted scan context: Global descriptor with sparse height feature for loop closure detection,” in *2021 International Conference on Computer, Control and Robotics (ICCCR)*. IEEE, 2021, pp. 214–219.
- [141] S. Lu, X. Xu, H. Yin, Z. Chen, R. Xiong, and Y. Wang, “One ring to rule them all: Radon sinogram for place recognition, orientation and translation estimation,” in *2022 IEEE/RSJ International Conference on Intelligent Robots and Systems (IROS)*, 2022, pp. 2778–2785.
- [142] X. Xu, S. Lu, J. Wu, H. Lu, Q. Zhu, Y. Liao, R. Xiong, and Y. Wang, “Ring++: Roto-translation invariant gram for global localization on a sparse scan map,” *arXiv preprint arXiv:2210.05984*, 2022.
- [143] W. Wang, H. Min, X. Wu, X. Hou, Y. Li, and X. Zhao, “High accuracy and low complexity lidar place recognition using unitary invariant frobenius norm,” *IEEE Sensors Journal*, 2022.
- [144] Y. Fan, X. Du, L. Luo, and J. Shen, “Fresco: Frequency-domain scan context for lidar-based place recognition with translation and rotation invariance,” in *2022 17th International Conference on Control, Automation, Robotics and Vision (ICARCV)*. IEEE, 2022, pp. 576–583.
- [145] F. Ou, Y. Li, and Z. Miao, “Place recognition of large-scale unstructured orchards with attention score maps,” *IEEE Robotics and Automation Letters*, 2023.
- [146] M. Magnusson, H. Andreasson, A. Nuchter, and A. J. Lilienthal, “Appearance-based loop detection from 3d laser data using the normal distributions transform,” in *2009 IEEE International Conference on Robotics and Automation*. IEEE, 2009, pp. 23–28.
- [147] J. Mo and J. Sattar, “A fast and robust place recognition approach for stereo visual odometry using lidar descriptors,” in *2020 IEEE/RSJ International Conference on Intelligent Robots and Systems (IROS)*. IEEE, 2020, pp. 5893–5900.
- [148] F. Cao, F. Yan, S. Wang, Y. Zhuang, and W. Wang, “Season-invariant and viewpoint-tolerant lidar place recognition in gps-denied environments,” *IEEE Transactions on Industrial Electronics*, vol. 68, no. 1, pp. 563–574, 2021.
- [149] L. He, X. Wang, and H. Zhang, “M2dp: A novel 3d point cloud descriptor and its application in loop closure detection,” in *2016 IEEE/RSJ International Conference on Intelligent Robots and Systems (IROS)*. IEEE, 2016, pp. 231–237.
- [150] L. Perdomo, D. Pittol, M. Mantelli, R. Maffei, M. Kolberg, and E. Prestes, “c-m2dp: A fast point cloud descriptor with color information to perform loop closure detection,” in *2019 IEEE 15th International Conference on Automation Science and Engineering (CASE)*. IEEE, 2019, pp. 1145–1150.
- [151] Y. Xia, Y. Xu, S. Li, R. Wang, J. Du, D. Cremers, and U. Stilla, “Soenet: A self-attention and orientation encoding network for point cloud based place recognition,” in *2021 IEEE/CVF Conference on Computer Vision and Pattern Recognition (CVPR)*. IEEE, 2021, pp. 11 343–11 352.
- [152] D. Cattaneo, M. Vaghi, and A. Valada, “Lcdnet: Deep loop closure detection and point cloud registration for lidar slam,” *IEEE Transactions on Robotics*, vol. 38, no. 4, pp. 2074–2093, 2022.
- [153] Z. Fan, H. Liu, J. He, Q. Sun, and X. Du, “Srnet: A 3d scene recognition network using static graph and dense semantic fusion,” in *Computer Graphics Forum*, vol. 39, no. 7. Wiley Online Library, 2020, pp. 301–311.
- [154] Z. Qiao, H. Hu, W. Shi, S. Chen, Z. Liu, and H. Wang, “A registration-aided domain adaptation network for 3d point cloud based place recognition,” in *2021 IEEE/RSJ International Conference on Intelligent Robots and Systems (IROS)*. IEEE, 2021, pp. 1317–1322.
- [155] L. Hui, H. Yang, M. Cheng, J. Xie, and J. Yang, “Pyramid point cloud transformer for large-scale place recognition,” in *Proceedings of the IEEE/CVF International Conference on Computer Vision*, 2021, pp. 6098–6107.
- [156] J. Komorowski, “Minkloc3d: Point cloud based large-scale place recognition,” in *Proceedings of the IEEE/CVF Winter Conference on Applications of Computer Vision*, 2021, pp. 1790–1799.
- [157] J. Komorowski, M. Wysoczańska, and T. Trzcinski, “Minkloc++: Lidar and monocular image fusion for place recognition,” in *2021 International Joint Conference on Neural Networks (IJCNN)*, 2021, pp. 1–8.
- [158] J. Komorowski, M. Wysoczańska, and T. Trzcinski, “Egonn: Ego-centric neural network for point cloud based 6dof relocalization at the city scale,” *IEEE Robotics and Automation Letters*, vol. 7, no. 2, pp. 722–729, 2021.
- [159] T.-X. Xu, Y.-C. Guo, Y.-K. Lai, and S.-H. Zhang, “Transloc3d: Point cloud based large-scale place recognition using adaptive receptive fields,” *arXiv preprint arXiv:2105.11605*, 2021.
- [160] J. Komorowski, “Improving point cloud based place recognition with ranking-based loss and large batch training,” in *2022 26th International Conference on Pattern Recognition (ICPR)*. IEEE, 2022, pp. 3699–3705.
- [161] K. Żywanowski, A. Banaszczyk, M. R. Nowicki, and J. Komorowski, “Minkloc3d-si: 3d lidar place recognition with sparse convolutions, spherical coordinates, and intensity,” *IEEE Robotics and Automation Letters*, vol. 7, no. 2, pp. 1079–1086, 2022.
- [162] K. Vidanapathirana, M. Ramezani, P. Moghadam, S. Sridharan, and C. Fookes, “Logg3d-net: Locally guided global descriptor learning for 3d place recognition,” in *2022 International Conference on Robotics and Automation (ICRA)*. IEEE, 2022, pp. 2215–2221.
- [163] M. Y. Chang, S. Yeon, S. Ryu, and D. Lee, “Spoxelnet: Spherical voxel-based deep place recognition for 3d point clouds of crowded indoor spaces,” in *2020 IEEE/RSJ International Conference on Intelligent Robots and Systems (IROS)*. IEEE, 2020, pp. 8564–8570.
- [164] S. Siva, Z. Nahman, and H. Zhang, “Voxel-based representation learning for place recognition based on 3d point clouds,” in *2020 IEEE/RSJ International Conference on Intelligent Robots and Systems (IROS)*, 2020, pp. 8351–8357.
- [165] Z. Hou, Y. Yan, C. Xu, and H. Kong, “Hitpr: Hierarchical transformer for place recognition in point cloud,” in *2022 International Conference on Robotics and Automation (ICRA)*. IEEE, 2022, pp. 2612–2618.
- [166] Z. Zhou, C. Zhao, D. Adolfsson, S. Su, Y. Gao, T. Duckett, and L. Sun, “Ndt-transformer: Large-scale 3d point cloud localisation using the normal distribution transform representation,” in *2021 IEEE International Conference on Robotics and Automation (ICRA)*. IEEE, 2021, pp. 5654–5660.
- [167] H. Yin, X. Ding, L. Tang, Y. Wang, and R. Xiong, “Efficient 3d lidar based loop closing using deep neural network,” in *2017 IEEE International Conference on Robotics and Biomimetics (ROBIO)*. IEEE, 2017, pp. 481–486.
- [168] D. Kong, X. Li, Y. Cen, Q. Xu, and A. Wang, “Simultaneous viewpoint- and condition-invariant loop closure detection based on lidar descriptor for outdoor large-scale environments,” *IEEE Transactions on Industrial Electronics*, vol. 70, no. 2, pp. 2117–2127, 2023.
- [169] J. Ma, X. Chen, J. Xu, and G. Xiong, “Seqot: A spatial-temporal transformer network for place recognition using sequential lidar data,” *IEEE Transactions on Industrial Electronics*, 2022.
- [170] J. Ma, J. Zhang, J. Xu, R. Ai, W. Gu, and X. Chen, “Overlap-transformer: An efficient and yaw-angle-invariant transformer network for lidar-based place recognition,” *IEEE Robotics and Automation Letters*, vol. 7, no. 3, pp. 6958–6965, 2022.
- [171] T. Barros, L. Garrote, R. Pereira, C. Premebida, and U. J. Nunes, “Attdlnet: Attention-based dl network for 3d lidar place recognition,” *arXiv preprint arXiv:2106.09637*, 2021.
- [172] Y. Lu, F. Yang, F. Chen, and D. Xie, “Pic-net: Point cloud and image collaboration network for large-scale place recognition,” *arXiv preprint arXiv:2008.00658*, 2020.
- [173] L. Bernreiter, L. Ott, J. Nieto, R. Siegwart, and C. Cadena, “Spherical multi-modal place recognition for heterogeneous sensor systems,” in *2021 IEEE International Conference on Robotics and Automation (ICRA)*. IEEE, 2021, pp. 1743–1750.
- [174] H. Lai, P. Yin, and S. Scherer, “Adafusion: Visual-lidar fusion with adaptive weights for place recognition,” *IEEE Robotics and Automation Letters*, vol. 7, no. 4, pp. 12 038–12 045, 2022.
- [175] M. Frosi and M. Matteucci, “Art-slam: Accurate real-time 6dof lidar slam,” *IEEE Robotics and Automation Letters*, vol. 7, no. 2, pp. 2692–2699, 2022.
- [176] L. Liao, C. Fu, B. Feng, and T. Su, “Optimized sc-f-loam: Optimized fast lidar odometry and mapping using scan context,” in *2022 6th CAA International Conference on Vehicular Control and Intelligence (CVCI)*, 2022, pp. 1–6.
- [177] W. Chen, Y. Wang, H. Chen, and Y. Liu, “Eil-slam: Depth-enhanced edge-based infrared-lidar slam,” *Journal of Field Robotics*, vol. 39, no. 2, pp. 117–130, 2022.

- [178] M. Magnusson, T. P. Kucner, S. G. Shahbandi, H. Andreasson, and A. J. Lilienthal, "Semi-supervised 3d place categorisation by descriptor clustering," in *2017 IEEE/RSJ International Conference on Intelligent Robots and Systems (IROS)*. IEEE, 2017, pp. 620–625.
- [179] Q. Meng, H. Guo, X. Zhao, D. Cao, and H. Chen, "Loop-closure detection with a multiresolution point cloud histogram mode in lidar odometry and mapping for intelligent vehicles," *IEEE/ASME Transactions on Mechatronics*, vol. 26, no. 3, pp. 1307–1317, 2021.
- [180] S. Chopra, R. Hadsell, and Y. LeCun, "Learning a similarity metric discriminatively, with application to face verification," in *2005 IEEE Computer Society Conference on Computer Vision and Pattern Recognition (CVPR'05)*, vol. 1. IEEE, 2005, pp. 539–546.
- [181] S. Shi, C. Guo, L. Jiang, Z. Wang, J. Shi, X. Wang, and H. Li, "Pv-rnn: Point-voxel feature set abstraction for 3d object detection," in *Proceedings of the IEEE/CVF Conference on Computer Vision and Pattern Recognition*, 2020, pp. 10 529–10 538.
- [182] F. Groh, P. Wiescholke, and H. P. Lensch, "Flex-convolution: Million-scale point-cloud learning beyond grid-worlds," in *Computer Vision—ACCV 2018: 14th Asian Conference on Computer Vision, Perth, Australia, December 2–6, 2018, Revised Selected Papers, Part I 14*. Springer, 2019, pp. 105–122.
- [183] J. Hu, L. Shen, and G. Sun, "Squeeze-and-excitation networks," in *Proceedings of the IEEE conference on computer vision and pattern recognition*, 2018, pp. 7132–7141.
- [184] T.-Y. Lin, P. Dollár, R. Girshick, K. He, B. Hariharan, and S. Belongie, "Feature pyramid networks for object detection," in *Proceedings of the IEEE conference on computer vision and pattern recognition*, 2017, pp. 2117–2125.
- [185] T.-Y. Lin, P. Dollár, R. Girshick, K. He, B. Hariharan, and S. Belongie, "Feature pyramid networks for object detection," in *Proceedings of the IEEE conference on computer vision and pattern recognition*, 2017, pp. 2117–2125.
- [186] H. Tang, Z. Liu, S. Zhao, Y. Lin, J. Lin, H. Wang, and S. Han, "Searching efficient 3d architectures with sparse point-voxel convolution," in *Computer Vision—ECCV 2020: 16th European Conference, Glasgow, UK, August 23–28, 2020, Proceedings, Part XXVIII*. Springer, 2020, pp. 685–702.
- [187] T.-L. Habich, M. Stuede, M. Labbé, and S. Spindeldreier, "Have i been here before? learning to close the loop with lidar data in graph-based slam," in *2021 IEEE/ASME International Conference on Advanced Intelligent Mechatronics (AIM)*. IEEE, 2021, pp. 504–510.
- [188] K. Granström and T. B. Schön, "Learning to close the loop from 3d point clouds," in *2010 IEEE/RSJ International Conference on Intelligent Robots and Systems*, 2010, pp. 2089–2095.
- [189] Y. Freund and R. E. Schapire, "A decision-theoretic generalization of on-line learning and an application to boosting," *Journal of computer and system sciences*, vol. 55, no. 1, pp. 119–139, 1997.
- [190] K. He, X. Zhang, S. Ren, and J. Sun, "Deep residual learning for image recognition," in *2016 IEEE Conference on Computer Vision and Pattern Recognition (CVPR)*, 2016, pp. 770–778.
- [191] T. S. Cohen, M. Geiger, J. Köhler, and M. Welling, "Spherical cnns," *arXiv preprint arXiv:1801.10130*, 2018.
- [192] C. Esteves, C. Allen-Blanchette, A. Makadia, and K. Daniilidis, "Learning so (3) equivariant representations with spherical cnns," in *Proceedings of the European Conference on Computer Vision (ECCV)*, 2018, pp. 52–68.
- [193] N. Perraudin, M. Defferrard, T. Kacprzak, and R. Sgier, "Deep-sphere: Efficient spherical convolutional neural network with healpix sampling for cosmological applications," *Astronomy and Computing*, vol. 27, pp. 130–146, 2019.
- [194] P. Besl and N. D. McKay, "A method for registration of 3-d shapes," *IEEE Transactions on Pattern Analysis and Machine Intelligence*, vol. 14, no. 2, pp. 239–256, 1992.
- [195] R. Dube, A. Cramariuc, D. Dugas, J. Nieto, R. Siegwart, and C. Cadena, "Segmap: 3d segment mapping using data-driven descriptors," in *Robotics: Science and Systems*, 2018.
- [196] K. Vidanapathirana, P. Moghadam, B. Harwood, M. Zhao, S. Sridharan, and C. Fookes, "Locus: Lidar-based place recognition using spatiotemporal higher-order pooling," in *2021 IEEE International Conference on Robotics and Automation (ICRA)*. IEEE, 2021, pp. 5075–5081.
- [197] M. A. Fischler and R. C. Bolles, "Random sample consensus: a paradigm for model fitting with applications to image analysis and automated cartography," *Communications of the ACM*, vol. 24, no. 6, pp. 381–395, 1981.
- [198] R. Dubé, M. G. Gollub, H. Sommer, I. Gilitschenski, R. Siegwart, C. Cadena, and J. Nieto, "Incremental-segment-based localization in 3-d point clouds," *IEEE Robotics and Automation Letters*, vol. 3, no. 3, pp. 1832–1839, 2018.
- [199] X. Ji, L. Zuo, C. Zhang, and Y. Liu, "Lloam: Lidar odometry and mapping with loop-closure detection based correction," in *2019 IEEE International Conference on Mechatronics and Automation (ICMA)*. IEEE, 2019, pp. 2475–2480.
- [200] R. Dubé, A. Gawel, H. Sommer, J. Nieto, R. Siegwart, and C. Cadena, "An online multi-robot slam system for 3d lidars," in *2017 IEEE/RSJ International Conference on Intelligent Robots and Systems (IROS)*, 2017, pp. 1004–1011.
- [201] J. Li, J. Zhao, Y. Kang, X. He, C. Ye, and L. Sun, "Dl-slam: Direct 2.5d lidar slam for autonomous driving," in *2019 IEEE Intelligent Vehicles Symposium (IV)*, 2019, pp. 1205–1210.
- [202] Y. Xie, Y. Zhang, L. Chen, H. Cheng, W. Tu, D. Cao, and Q. Li, "Rdc-slam: A real-time distributed cooperative slam system based on 3d lidar," *IEEE Transactions on Intelligent Transportation Systems*, 2021.
- [203] Y. Gong, F. Sun, J. Yuan, W. Zhu, and Q. Sun, "A two-level framework for place recognition with 3d lidar based on spatial relation graph," *Pattern Recognition*, vol. 120, p. 108171, 2021.
- [204] Y. Fan, Y. He, and U.-X. Tan, "Seed: A segmentation-based egocentric 3d point cloud descriptor for loop closure detection," in *2020 IEEE/RSJ International Conference on Intelligent Robots and Systems (IROS)*. IEEE, 2020, pp. 5158–5163.
- [205] G. Tinchev, S. Nobili, and M. Fallon, "Seeing the wood for the trees: Reliable localization in urban and natural environments," in *2018 IEEE/RSJ International Conference on Intelligent Robots and Systems (IROS)*, 2018, pp. 8239–8246.
- [206] G. Tinchev, A. Penate-Sanchez, and M. Fallon, "Learning to see the wood for the trees: Deep laser localization in urban and natural environments on a cpu," *IEEE Robotics and Automation Letters*, vol. 4, no. 2, pp. 1327–1334, 2019.
- [207] Y. Li, R. Bu, M. Sun, W. Wu, X. Di, and B. Chen, "Pointcnn: Convolution on x-transformed points," in *NeurIPS*, 2018.
- [208] R. Dube, A. Cramariuc, D. Dugas, H. Sommer, M. Dymczyk, J. Nieto, R. Siegwart, and C. Cadena, "Segmap: Segment-based mapping and localization using data-driven descriptors," *The International Journal of Robotics Research*, vol. 39, no. 2-3, pp. 339–355, 2020.
- [209] D. Rozenberszki and A. L. Majdik, "Lol: Lidar-only odometry and localization in 3d point cloud maps," in *2020 IEEE International Conference on Robotics and Automation (ICRA)*, 2020, pp. 4379–4385.
- [210] A. Cramariuc, F. Tschopp, N. Alatur, S. Benz, T. Falck, M. Brühlmeier, B. Hahn, J. Nieto, and R. Siegwart, "Semsegmap-3d segment-based semantic localization," in *2021 IEEE/RSJ International Conference on Intelligent Robots and Systems (IROS)*. IEEE, 2021, pp. 1183–1190.
- [211] J. Wietrzykowski and P. Skrzypczyński, "On the descriptive power of lidar intensity images for segment-based loop closing in 3-d slam," in *2021 IEEE/RSJ International Conference on Intelligent Robots and Systems (IROS)*, 2021, pp. 79–85.
- [212] I. Bogoslavskyi and C. Stachniss, "Fast range image-based segmentation of sparse 3d laser scans for online operation," in *2016 IEEE/RSJ International Conference on Intelligent Robots and Systems (IROS)*, 2016, pp. 163–169.
- [213] J. Cui, Y. Cai, T. Huang, J. Zhao, L. Xiong, and Z. Yu, "Dsc: Deep scan context descriptor for large-scale place recognition," in *2022 IEEE International Conference on Multisensor Fusion and Integration for Intelligent Systems (MFI)*. IEEE, 2022, pp. 1–7.
- [214] A. Gawel, C. Del Don, R. Siegwart, J. Nieto, and C. Cadena, "X-view: Graph-based semantic multi-view localization," *IEEE Robotics and Automation Letters*, vol. 3, no. 3, pp. 1687–1694, 2018.
- [215] G. Pramatarov, D. De Martini, M. Gadd, and P. Newman, "Box-graph: Semantic place recognition and pose estimation from 3d lidar," *arXiv preprint arXiv:2206.15154*, 2022.
- [216] L. Li, X. Kong, X. Zhao, T. Huang, and Y. Liu, "Semantic scan context: a novel semantic-based loop-closure method for lidar slam," *Autonomous Robots*, vol. 46, no. 4, pp. 535–551, 2022.
- [217] A. Milioto, I. Vizzo, J. Behley, and C. Stachniss, "Rangenet++: Fast and accurate lidar semantic segmentation," in *2019 IEEE/RSJ international conference on intelligent robots and systems (IROS)*. IEEE, 2019, pp. 4213–4220.
- [218] H. Yuan, Y. Zhang, S. Fan, X. Li, and J. Wang, "Object scan context: Object-centric spatial descriptor for place recognition

- within 3d point cloud map," *arXiv preprint arXiv:2206.03062*, 2022.
- [219] A. Zaganidis, A. Zernitv, T. Duckett, and G. Cielniak, "Semantically assisted loop closure in slam using ndt histograms," in *2019 IEEE/RSJ International Conference on Intelligent Robots and Systems (IROS)*. IEEE, 2019, pp. 4562–4568.
- [220] M. Magnusson, H. Andreasson, A. Nuchter, and A. J. Lilienthal, "Automatic appearance-based loop detection from three-dimensional laser data using the normal distributions transform," *Journal of Field Robotics*, vol. 26, no. 11-12, pp. 892–914, 2009.
- [221] L. Li, X. Kong, X. Zhao, T. Huang, W. Li, F. Wen, H. Zhang, and Y. Liu, "Rinet: Efficient 3d lidar-based place recognition using rotation invariant neural network," *IEEE Robotics and Automation Letters*, vol. 7, no. 2, pp. 4321–4328, 2022.
- [222] L. Bernreiter, A. Gawel, H. Sommer, J. Nieto, R. Siegwart, and C. C. Lerma, "Multiple hypothesis semantic mapping for robust data association," *IEEE Robotics and Automation Letters*, vol. 4, no. 4, pp. 3255–3262, 2019.
- [223] X. Chen, T. Läbe, A. Milioto, T. Röhling, J. Behley, and C. Stachniss, "Overlapnet: a siamese network for computing lidar scan similarity with applications to loop closing and localization," *Autonomous Robots*, vol. 46, no. 1, pp. 61–81, 2022.
- [224] X. Chen, T. Läbe, L. Nardi, J. Behley, and C. Stachniss, "Learning an overlap-based observation model for 3d lidar localization," in *2020 IEEE/RSJ International Conference on Intelligent Robots and Systems (IROS)*, 2020, pp. 4602–4608.
- [225] P. Yin, L. Xu, Z. Feng, A. Egorov, and B. Li, "Pse-match: A viewpoint-free place recognition method with parallel semantic embedding," *IEEE Transactions on Intelligent Transportation Systems*, 2021.
- [226] D. Dai, J. Wang, Z. Chen, and P. Bao, "Sc-lpr: Spatiotemporal context based lidar place recognition," *Pattern Recognition Letters*, vol. 156, pp. 160–166, 2022.
- [227] K. Ebadi, Y. Chang, M. Palieri, A. Stephens, A. Hatteland, E. Heiden, A. Thakur, N. Funabiki, B. Morrell, S. Wood, L. Carlone, and A.-a. Agha-mohammadi, "Lamp: Large-scale autonomous mapping and positioning for exploration of perceptually-degraded subterranean environments," in *2020 IEEE International Conference on Robotics and Automation (ICRA)*, 2020, pp. 80–86.
- [228] N. Rottmann, R. Bruder, A. Schweikard, and E. Rueckert, "Loop closure detection in closed environments," in *2019 European Conference on Mobile Robots (ECMR)*. IEEE, 2019, pp. 1–8.
- [229] C. Wen, Y. Dai, Y. Xia, Y. Lian, J. Tan, C. Wang, and J. Li, "Toward efficient 3-d colored mapping in gps-/gnss-denied environments," *IEEE Geoscience and Remote Sensing Letters*, vol. 17, no. 1, pp. 147–151, 2020.
- [230] B. Zhou, Y. He, K. Qian, X. Ma, and X. Li, "S4-slam: A real-time 3d lidar slam system for ground/watersurface multi-scene outdoor applications," *Autonomous Robots*, vol. 45, no. 1, pp. 77–98, 2021.
- [231] E. Mendes, P. Koch, and S. Lacroix, "Icp-based pose-graph slam," in *2016 IEEE International Symposium on Safety, Security, and Rescue Robotics (SSRR)*. IEEE, 2016, pp. 195–200.
- [232] C. Le Gentil, T. Vidal-Calleja, and S. Huang, "In2laama: Inertial lidar localization autocalibration and mapping," *IEEE Transactions on Robotics*, vol. 37, no. 1, pp. 275–290, 2020.
- [233] J. Jiang, J. Wang, P. Wang, P. Bao, and Z. Chen, "Lipmatch: Lidar point cloud plane based loop-closure," *IEEE Robotics and Automation Letters*, vol. 5, no. 4, pp. 6861–6868, 2020.
- [234] M. Yokozuka, K. Koide, S. Oishi, and A. Banno, "Litamin: Lidar-based tracking and mapping by stabilized icp for geometry approximation with normal distributions," in *2020 IEEE/RSJ International Conference on Intelligent Robots and Systems (IROS)*, 2020, pp. 5143–5150.
- [235] —, "Litamin2: Ultra light lidar-based slam using geometric approximation applied with kl-divergence," in *2021 IEEE International Conference on Robotics and Automation (ICRA)*. IEEE, 2021, pp. 11 619–11 625.
- [236] A. Segal, D. Haehnel, and S. Thrun, "Generalized-icp." in *Robotics: science and systems*, vol. 2, no. 4. Seattle, WA, 2009, p. 435.
- [237] J. G. Mangelson, D. Dominic, R. M. Eustice, and R. Vasudevan, "Pairwise consistent measurement set maximization for robust multi-robot map merging," in *2018 IEEE International Conference on Robotics and Automation (ICRA)*, 2018, pp. 2916–2923.
- [238] Y. Chang, K. Ebadi, C. E. Denniston, M. F. Ginting, A. Rosinol, A. Reinke, M. Palieri, J. Shi, A. Chatterjee, B. Morrell, A.-a. Agha-mohammadi, and L. Carlone, "Lamp 2.0: A robust multi-robot slam system for operation in challenging large-scale underground environments," *IEEE Robotics and Automation Letters*, vol. 7, no. 4, pp. 9175–9182, 2022.
- [239] H. Yang, J. Shi, and L. Carlone, "Teaser: Fast and certifiable point cloud registration," *IEEE Transactions on Robotics*, vol. 37, no. 2, pp. 314–333, 2021.
- [240] Z. Gong, J. Li, Z. Luo, C. Wen, C. Wang, and J. Zelek, "Mapping and semantic modeling of underground parking lots using a backpack lidar system," *IEEE Transactions on Intelligent Transportation Systems*, vol. 22, no. 2, pp. 734–746, 2021.
- [241] R. Kümmerle, G. Grisetti, H. Strasdat, K. Konolige, and W. Burgard, "g2o: A general framework for graph optimization," in *2011 IEEE International Conference on Robotics and Automation*. IEEE, 2011, pp. 3607–3613.
- [242] Z. Liu, C. Suo, S. Zhou, F. Xu, H. Wei, W. Chen, H. Wang, X. Liang, and Y.-H. Liu, "Seqlpd: Sequence matching enhanced loop-closure detection based on large-scale point cloud description for self-driving vehicles," in *2019 IEEE/RSJ International Conference on Intelligent Robots and Systems (IROS)*. IEEE, 2019, pp. 1218–1223.
- [243] M. J. Milford and G. F. Wyeth, "Seqslam: Visual route-based navigation for sunny summer days and stormy winter nights," in *2012 IEEE international conference on robotics and automation*. IEEE, 2012, pp. 1643–1649.
- [244] W. Chen, H. Zhao, Q. Shen, C. Xiong, S. Zhou, and Y.-H. Liu, "Inertial aided 3d lidar slam with hybrid geometric primitives in large-scale environments," in *2021 IEEE International Conference on Robotics and Automation (ICRA)*. IEEE, 2021, pp. 11 566–11 572.
- [245] P. Yin, L. Xu, J. Zhang, and H. Choset, "Fusionvlad: A multi-view deep fusion networks for viewpoint-free 3d place recognition," *IEEE Robotics and Automation Letters*, vol. 6, no. 2, pp. 2304–2310, 2021.
- [246] M. Aldibaja, N. Sukanuma, R. Yanase, L. Cao, K. Yoneda, and A. Kuramoto, "Loop-closure and map-combiner detection strategy based on lidar reflectance and elevation maps," in *2020 IEEE 23rd International Conference on Intelligent Transportation Systems (ITSC)*. IEEE, 2020, pp. 1–7.
- [247] I. A. Barsan, S. Wang, A. Pokrovsky, and R. Urtasun, "Learning to localize using a lidar intensity map," in *Conference on Robot Learning*. PMLR, 2018, pp. 605–616.
- [248] Y. Cho, G. Kim, S. Lee, and J.-H. Ryu, "Openstreetmap-based lidar global localization in urban environment without a prior lidar map," *IEEE Robotics and Automation Letters*, vol. 7, no. 2, pp. 4999–5006, 2022.
- [249] P. Shi, J. Li, and Y. Zhang, "A fast lidar place recognition and localization method by fusing local and global search," *ISPRS Journal of Photogrammetry and Remote Sensing*, vol. 202, pp. 637–651, 2023.
- [250] Z. Liu, H. Chen, H. Di, Y. Tao, J. Gong, G. Xiong, and J. Qi, "Real-time 6d lidar slam in large scale natural terrains for ugv," in *2018 IEEE Intelligent Vehicles Symposium (IV)*. IEEE, 2018, pp. 662–667.
- [251] H. Yin, L. Tang, X. Ding, Y. Wang, and R. Xiong, "Loconet: Global localization in 3d point clouds for mobile vehicles," in *2018 IEEE Intelligent Vehicles Symposium (IV)*. IEEE, 2018, pp. 728–733.
- [252] L. Sun, D. Adolffson, M. Magnusson, H. Andreasson, I. Posner, and T. Duckett, "Localising faster: Efficient and precise lidar-based robot localisation in large-scale environments," in *2020 IEEE International Conference on Robotics and Automation (ICRA)*. IEEE, 2020, pp. 4386–4392.
- [253] Y. Jin, Q. Chen, J. Qian, J. Liu, and J. Zhang, "Global localization for single 3d point cloud using voting mechanism," in *2021 6th IEEE International Conference on Advanced Robotics and Mechatronics (ICARM)*. IEEE, 2021, pp. 771–776.
- [254] B. Zhou, Y. He, W. Huang, X. Yu, F. Fang, and X. Li, "Place recognition and navigation of outdoor mobile robots based on random forest learning with a 3d lidar," *Journal of Intelligent & Robotic Systems*, vol. 104, no. 4, pp. 1–26, 2022.
- [255] P. Ruchti, B. Steder, M. Ruhnke, and W. Burgard, "Localization on openstreetmap data using a 3d laser scanner," in *2015 IEEE international conference on robotics and automation (ICRA)*. IEEE, 2015, pp. 5260–5265.
- [256] B. Suger and W. Burgard, "Global outer-urban navigation with openstreetmap," in *2017 IEEE International Conference on Robotics and Automation (ICRA)*. IEEE, 2017, pp. 1417–1422.
- [257] F. Yan, O. Vysotska, and C. Stachniss, "Global localization on openstreetmap using 4-bit semantic descriptors," in *2019 European Conference on Mobile Robots (ECMR)*. IEEE, 2019, pp. 1–7.

- [258] J. Behley and C. Stachniss, "Efficient surfel-based slam using 3d laser range data in urban environments." in *Robotics: Science and Systems*, vol. 2018, 2018, p. 59.
- [259] P. Yin, L. Xu, Z. Liu, L. Li, H. Salman, Y. He, W. Xu, H. Wang, and H. Choset, "Stabilize an unsupervised feature learning for lidar-based place recognition," in *2018 IEEE/RSJ International Conference on Intelligent Robots and Systems (IROS)*. IEEE, 2018, pp. 1162–1167.
- [260] K. He, X. Zhang, S. Ren, and J. Sun, "Deep residual learning for image recognition," in *Proceedings of the IEEE conference on computer vision and pattern recognition*, 2016, pp. 770–778.
- [261] G. Pandey, J. R. McBride, and R. M. Eustice, "Ford campus vision and lidar data set," *The International Journal of Robotics Research*, vol. 30, no. 13, pp. 1543–1552, 2011.
- [262] A. Geiger, P. Lenz, and R. Urtasun, "Are we ready for autonomous driving? the kitti vision benchmark suite," in *2012 IEEE Conference on Computer Vision and Pattern Recognition*, 2012, pp. 3354–3361.
- [263] N. Carlevaris-Bianco, A. K. Ushani, and R. M. Eustice, "University of michigan north campus long-term vision and lidar dataset," *The International Journal of Robotics Research*, vol. 35, no. 9, pp. 1023–1035, 2016.
- [264] W. Maddern, G. Pascoe, C. Linegar, and P. Newman, "1 year, 1000 km: The oxford robotcar dataset," *The International Journal of Robotics Research*, vol. 36, no. 1, pp. 3–15, 2017.
- [265] J. Jeong, Y. Cho, Y.-S. Shin, H. Roh, and A. Kim, "Complex urban lidar data set," in *2018 IEEE International Conference on Robotics and Automation (ICRA)*, 2018, pp. 6344–6351.
- [266] J. Behley, M. Garbade, A. Milioto, J. Quenzel, S. Behnke, C. Stachniss, and J. Gall, "Semantickitti: A dataset for semantic scene understanding of lidar sequences," in *Proceedings of the IEEE/CVF International Conference on Computer Vision*, 2019, pp. 9297–9307.
- [267] G. Kim, Y. S. Park, Y. Cho, J. Jeong, and A. Kim, "Mulran: Multimodal range dataset for urban place recognition," in *2020 IEEE International Conference on Robotics and Automation (ICRA)*, 2020, pp. 6246–6253.
- [268] W. Zhou, J. S. Berrio, C. De Alvis, M. Shan, S. Worrall, J. Ward, and E. Nebot, "Developing and testing robust autonomy: The university of sydney campus data set," *IEEE Intelligent Transportation Systems Magazine*, vol. 12, no. 4, pp. 23–40, 2020.
- [269] D. Barnes, M. Gadd, P. Murcutt, P. Newman, and I. Posner, "The oxford radar robotcar dataset: A radar extension to the oxford robotcar dataset," in *2020 IEEE International Conference on Robotics and Automation (ICRA)*. IEEE, 2020, pp. 6433–6438.
- [270] Y. Liao, J. Xie, and A. Geiger, "Kitti-360: A novel dataset and benchmarks for urban scene understanding in 2d and 3d," *IEEE Transactions on Pattern Analysis and Machine Intelligence*, 2022.
- [271] J. Knights, P. Moghadam, M. Ramezani, S. Sridharan, and C. Fookes, "Includ: Incremental learning for point cloud place recognition," in *2022 IEEE/RSJ International Conference on Intelligent Robots and Systems (IROS)*. IEEE, 2022, pp. 8559–8566.
- [272] D. Gálvez-López and J. D. Tardos, "Bags of binary words for fast place recognition in image sequences," *IEEE Transactions on Robotics*, vol. 28, no. 5, pp. 1188–1197, 2012.
- [273] B. Ferrarini, M. Waheed, S. Waheed, S. Ehsan, M. J. Milford, and K. D. McDonald-Maier, "Exploring performance bounds of visual place recognition using extended precision," *IEEE Robotics and Automation Letters*, vol. 5, no. 2, pp. 1688–1695, 2020.